Applied Thermal Engineering 265 (2025) 125606

Contents lists available at ScienceDirect

Applied Thermal Engineering

journal homepage: www.elsevier.com/locate/apthermeng

Research Paper

Latent heat thermal energy storage system with pillow-plate heat exchangers topology – Assessment of thermo-fluid dynamic performance and application potential☆

Pouriya H. Niknam, Lorenzo Ciappi, Adriano Sciacovelli

School of Chemical Engineering University of Birmingham UK

ARTICLE INFO

Keywords:
Thermal energy storage
Waste heat recovery
Topology
PCM Phase Change Materials
Numerical modelling
Decarbonization

ABSTRACT

This research investigates the novel concept of pillow plate latent heat thermal energy storage (PP-LHTES) for storing process heat and/or waste heat at medium temperature, up to around 200 °C, and with a focus on mobile TES applications, such those in the maritime sector. The work introduces a novel methodology that combines computational fluid dynamics (CFD) with reduced-order modelling (ROM) techniques to evaluate the thermo-economic performance of PP-LHTES at the prototype scale (~102 kWh) and predict its potential at full scale (~MWh). These are the key aspects of novelty of the research. The study focuses on the impact of key technical factors, including the selection and thermophysical properties of the phase change material (PCM), its melting temperature and latent heat of fusion, the operating temperature, and the flow rate of the heat transfer fluid. Furthermore, the cost-effectiveness of PP-LHTES was examined by evaluating nine design parameters, such as the number of pillow plates and the cost per unit of PCM. Findings indicate that PP-LHTES appear to have a competitive advantage in volumetric energy storage density at the system level (~89 kWh/m^3), making it more compact than other LHTES solutions (~53 kWh/m^3) with a similar specific capital cost (~200 €/kWh). The PP-LHTES module weighs 500 kg, occupies 0.25 m^3, and provides an energy storage capacity of 17 to 22 kWh. The scalability of the design is investigated and results emphasize the its versatility. The mass-averaged volumetric energy storage density is comparable to existing LHTES systems (~50 kWh/t). This is due to the distinctive design of pillow plate heat exchangers, which integrate heat transfer fluid channels and extended heat transfer surfaces into a compact structure. This design increases energy density at the system level, reduces the overall footprint, and enhances the feasibility of deploying TES devices in end-user applications.

1. Introduction

The transition from non-renewable to zero-carbon and efficient energy generation and utilisation remains the uppermost critical challenge across all societal sectors. Within this context, the maritime sector needs further energy efficiency enhancements, given the commitment of the International Maritime Organisation (IMO) to achieving net zero greenhouse gas (GHG) emissions by 2050. The goal is set against projections of an increase in emissions between 50 % and 250 % by 2050, if unaddressed, due to increased maritime transportation [1]. This highlights the critical need for both technological advancements and operational optimisations.

Technological innovations play a central role in reducing GHG emissions from ships, through improvements in engine efficiency and the integration of new energy technologies. Strategies to enhance energy efficiency encompass refining propulsion systems, increasing the utilisation of renewable energy for electricity, and adopting waste heat recovery (WHR) technologies [2,3]. For what concerns propulsion systems, the maritime sector remains dominated by ships propelled by diesel engines with the levels of waste heat (WH) accounting for 50 % or more of primary energy provided by fuel [4]. Thus, efforts are focused on switching towards cleaner alternatives like LNG, methanol, hydrogen, and ammonia [3,5,6,7] as well as wind-assisted propulsion [8].

Nonetheless, waste heat recovery (WHR) remains a crucial strategy in augmenting on-board energy efficiency, with potential fuel consumption reductions estimated between 3 % and 15 % [9,10]. Although mature WHR technologies, such as waste heat boilers and turbocharging systems are fully deployed on ships [3,5], emerging WHR technologies

☆ This article is part of a special issue entitled: 'HPC2023' published in Applied Thermal Engineering.

E-mail address: a.sciacovelli@bham.ac.uk (A. Sciacovelli).

https://doi.org/10.1016/j.applthermaleng.2025.125606
Received 11 April 2024; Received in revised form 28 November 2024; Accepted 15 January 2025
Available online 18 January 2025

Nomenclature

Roman symbols

A	Area [m^2]
A_M	Mushy zone constant, [-]
B	Melt fraction, [-]
C_p	Constant pressure specific heat [J/kg/K]
D_e	Pipe diameter [mm]
D_p	Plate pipe diameter [mm]
D_{we}	Welding external diameter [mm]
D_{wi}	Welding internal diameter [mm]
E	Specific energy [J/m^3]
g	Gravitational acceleration [m/s^2]
H	Specific total enthalpy [J/kg]
h	Specific sensible enthalpy [J/kg]
h	hour
K	Thermal conductivity [W/m/K]
k	Effective thermal conductivity [W/m/K]
L	Specific latent heat [J/kg]
$\dot{m}$	Mass flow rate [kg/s]
n_p	Plate number [-]
n_w	Welding number [-]
p	Pressure [Pa]
q	Heat flux [W/m^2]
S_{en}	Energy source term [$J/s/m^3$]
S_{mo}	Momentum sink [m/s]
T	Temperature [K]
T_A	Surface adjacent air temperature [K]
T_S	Surface temperature [K]
T_s	Source or sink temperature [K]
v	Velocity vector [m/s]
$\mathbf{v}_p$	Pull velocity vector [m/s]
t	Time [s]

Greek symbols

β	Liquid volume fraction [-]
ε	Mathematical constant [-]
ρ	Density [kg/m^3]

Other symbols

Δt	Time step [s]
Δx	Finite difference layer thickness [m]

Acronyms

Cap	Capacity
CFD	Computational fluid dynamics
CT	Cycle Time
ED	Energy density
HE	Heat exchanger
HTF	Heat transfer fluid
IMO	International Maritime Organisation
KPI	Key Performance Indicator
LHS	Latin hypercube sampling
LHTES	Latent heat thermal energy storage
LNG	Liquefied natural gas
ORC	Organic Rankine cycle
PCM	Phase change material
PP	Pillow plate
STHE	Shell and tube heat exchanger
TES	Thermal energy storage
TEU	Standard twenty-foot container
URANS	Unsteady Reynolds averaged Navier-Stokes
WHR	Waste heat recovery

from terrestrial applications still present significant opportunities for enhancement and integration into on-board applications. The overarching challenges lie in maximising WH recovery, particularly at the low and intermediate levels of temperature, while concurrently mitigating the intermittency of waste heat availability [3,11]. In this regard, advanced WHR solutions, including among others, organic Rankine cycles (ORC) [12,13], isobaric expansion engines (IEE) [14], sorption cooling systems [15] and thermal energy storage (TES) [16,17], not only convert and valorise WH but also address the intermittency of on-board demands, particularly on passenger vessels as cruise ships [13,18,19].

In this context, the exploration of thermal energy storage (TES) systems for maritime applications remains substantially limited, with only few studies addressing such technology in the maritime context [18,19]. Scope for on-board TES emerges from the intermittent nature of WH and thermal demand on ships driven by variable ship operational profiles such as cruising, hoteling, and harbour manoeuvring [13,18,19], which identify the necessity for dedicated research into bespoke TES solutions. This paper addresses such needs by proposing and assessing an innovative TES device, specifically tailored for reduced footprint and integration with WHR systems operating at low or intermediate levels of temperature.

The present research focuses on latent heat thermal energy storage (LHTES) systems in the context of the utilisation of mid-to-low-temperature waste heat sources on ships, which is currently unaddressed compared to high-temperature sources. These systems exploit the phase transition of phase change materials (PCMs) between liquid and solid to store thermal energy, offering substantial capabilities even with minimal temperature differences [20,21,22]. Recent advancements in LHTES technology aimed at minimising the physical footprint, reducing costs, and optimising the duration of thermal charge and discharge cycles through enhanced heat exchange designs and mechanisms exchange [20,21,22]. These targets can be achieved through the specific design of the geometry of the heat exchanger (HE) and the choice of the most suited phase change material (PCM) for the conditions of the heat transfer fluid (HTF). However, so far, only a very limited number of studies focused on the development of on-board LHTES systems. Exemplary cases include the work of Frazzica et al. who developed and tested a hybrid TES device for on-board applications exploiting the sensible and latent heat of PCM macro-capsules contained in a vertical sensible tank, achieving an overall storage density of up to 35 % higher than conventional sensible TES devices [23]. Similarly, Catapano et al. realised a small-scale prototype of the WHR system embedding a Stirling engine an ORC device and a LHTES device and tested it under conditions resembling the functioning of a ship during winter and summer cruises, obtaining a recovery of thermal energy of 7.7 % of the total fuel energy [24]. Moreover, Godiff developed a CFD model of an LHTES tank of a downscaled naval system investigating the effects of the use of diverse PCMs on waste heat recovery [25]. In addition, Zhang et al. applied a mathematical model of a WHR system integrated with a latent thermal energy storage unit for a vessel application achieving an increase of 7.9 % of the recovered heat compared to traditional solutions [25].

Further numerical investigations were conducted by Ye et al. on different typologies of phase change materials. Firstly, they identified and clarified mechanisms behind convective false diffusion for enthalpy-porosity modelling of the solid–liquid interface in pure solid-gallium melting, analysed the asymmetrical solid–liquid interface, and proposed fitting correlations regarding equilibrium state during phase change [26]. Then, they proposed a correlation for calculating the mean liquid layer thickness for the phase change of pure solid-gallium using the enthalpy-porosity methodology and studied the irregular interface shapes caused by the highly anisotropic properties of solid crystal

gallium [27]. Finally, they developed a correlation for the dimensionless mushy zone constant in terms of the Exploring mushy zone constant Grashof number and Stefan number based on enthalpy-porosity modelling [28].

Further, common to the existing studies on LHTES for naval applications, is the adoption of off-the-shelf designs, chiefly finned shell-and-tube LHTES. A wide variety of literature references investigated these systems by applying analytical [29,30,31], CFD [32,33,34] and experimental [35,36,37] models. Alternative innovative designs instead remain largely unexplored.

1.1. Novelty

Overall, from the literature studies discussed above, it emerges that the development and understanding of alternative LHTES technological solutions remain limited, particularly for applications in sectors such difficult to decarbonise as the maritime sector. This work specifically addresses this need by investigating an alternative topology of LHTES systems based on the pillow plate heat exchanger (PP-HE) technology and tailored for the storage of mid-temperature waste heat (up to ~ 200 °C), both of which are the key novelties of the work. Indeed, their current understanding remains confined to a limited number of studies either focusing on empirically-based assessments [38,39] or simplified parametric studies [40].

A study was conducted on a TES device for on-board applications with thermal evaluation of the charge and discharge thermal cycles by applying a CFD model. The effects on performance of the latent heat and melting temperature of PCM (80–130 °C), the fluid dynamics of HTF, and the temperature of source and sink (50–160 °C) were investigated [41]. The present work aims at expanding and reinforcing the knowledge of these aspects through the following novel contributions to the existing body of literature.

- Comprehensive performance assessment underpinned by a novel approach combining computational fluid dynamic (CFD) tailored for PP-LHTES with reduced-order modelling (ROM) to extensively ascertain the impact of PCM selection, operating temperature and HTF flow rate on PP-LHTES thermo-fluid performance.
- Bottom-up understanding of the economic feasibility of PP-LHTES through an economic analysis which complements the thermo-fluid performance assessment by scrutinising the influence of the key cost components such as PCM, PP-HE and HTF on the expected cost of the whole PP-LHTES system.
- Understanding of the potential for PP-LHTES to scale up towards future applications in a realistic environment at a scale of MWh for the rated energy.

In doing so, this work represents a first-of-a-kind analysis of the performance and potential of PP-LHTES devices. Ultimately, it contributes to exploring and advancing the development of LHTES technology by strengthening the understanding of a novel concept with currently untapped potential in attaining competitive thermo-economic performance in the considered application context.

2. Pillow plate latent thermal energy storage

According to the literature, various waste heat streams are present within on-board energy systems, predominantly associated with the vessel's propulsion system. There are intrinsic differences in both the quantity and characteristics of these sources. The predominant form of available waste heat arises from exhaust gases emitted by the main engine, auxiliary engines, or boilers, all of which are typically fuelled by fossil-fuel combustion.

The heat associated with the exhaust accounts for up to 28 % of the fuel energy, and the temperature is reported within 200 °C to 360 °C. Both high quantity and high temperature turn the exhaust gas into a great opportunity for WHR technologies. Another major WH source is the scavenging air. The high quantity along with the temperature of the exhaust gas led to high potential for waste heat recovery. In addition, there is scavenging air which is used to remove post-combustion gases from the engine, thereby requiring cooling and some heat would be available for recovery. It accounts for up to 16 % of the fuel energy, and temperature below 200 °C exiting the engine. The quantity and temperature level still provide favourable conditions for WHR. Alternative sources on board are the jacket water and lubricating oil, each roughly accounting for 5 % of fuel energy, and temperatures are below 100 °C. The characterisation summary of on-board WH sources and the overlap is roughly demonstrated in Fig. 1 [42,43,44,45]. In addition to quantity and temperature, the level of availability of WH sources also impacts the overall WH. Upon continuous availability of WH, as the exhaust during the vessel cruising at consistent speed, a relatively constant WH would be available, thereby integrating WHR technologies can play a role for uninterrupted energy conversion and turning WH into a useful form of energy. Another part of the WH stems from the inconsistency of operational state of the on-board energy system, resulting in having a variable and intermittent WH. Such parts of the WH are a great opportunity for the deployment of Thermal energy storage, buffering the variable WH for delivery in more stable condition, fulfilling the heat demand or alternatives. The WH quality, quantity, and availability all associated with the type of vessel and characteristics of the journey, however, the design of LHTES solutions in the present study is aligned with a reasonable range of WH temperatures and vessel characteristics.

Thermal energy storage devices based on phase change material have two principal functions: they mitigate the fluctuations of demand and supply of thermal energy, and they accumulate and release thermal energy [46]. In particular, the configuration of these devices using pillow plates is illustrated in Fig. 2. It is a heat exchanger composed of a set of plates stacked parallel to each other in the horizontal direction. The plate bundle allows the circulation of the heat transfer fluid in the system and is surrounded by a phase change material that acts as a heat storage medium. Both the pillow plate bundle and the PCM are contained in a tank. Two manifolds connect all the plates with direct joints and the inlet or outlet pipes with the circuit of the heat transfer fluid.

The peculiar component of these devices is the pillow plate (PP), which consists of two metallic plates with the same wall thickness that are spot-welded together creating an internal pattern and that are sealed with a welded seam along their contours. The plates are expanded by inflation, in one or two directions, until the desired height for the

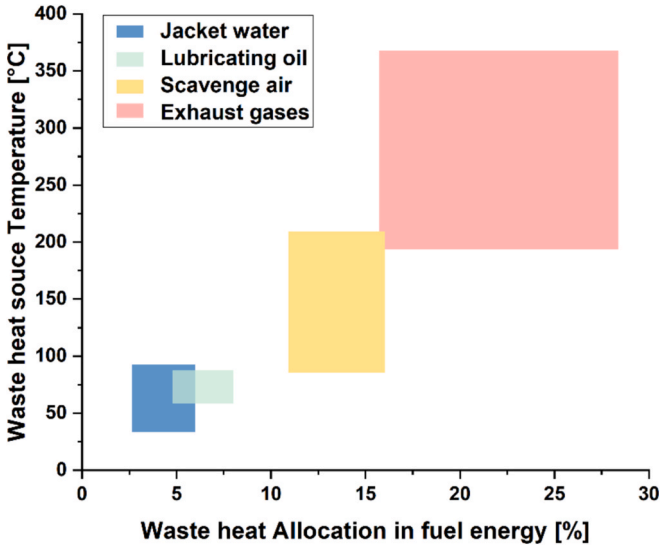

Fig. 1. The temperature and amount of waste heat sources on board ships [42,43,44,45].

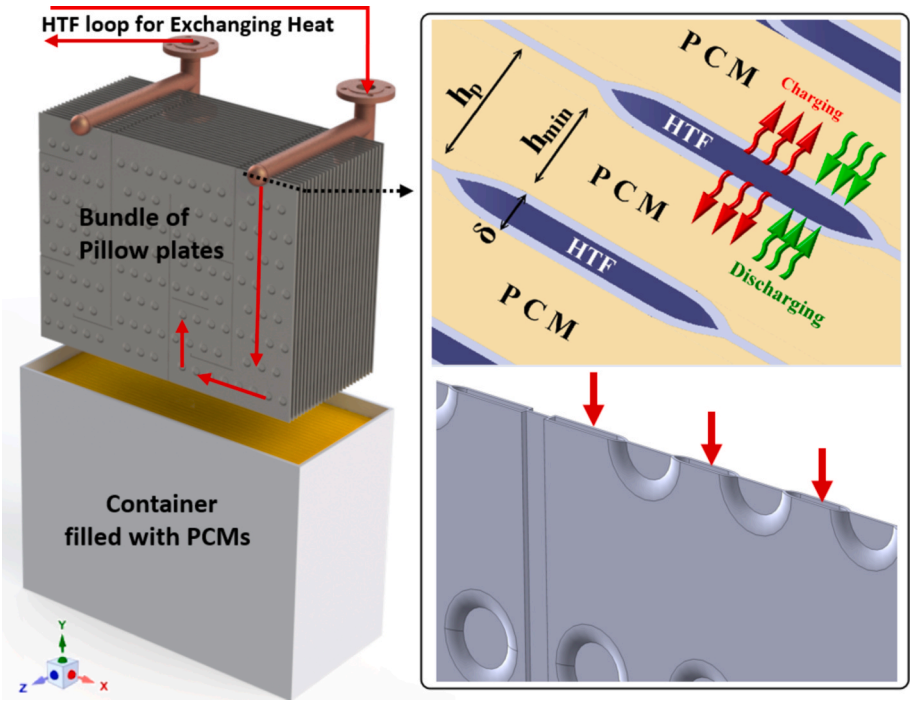

Fig. 2. Proposed configuration of the PP-LHTES system.

passage of the HTF is obtained. The PP-HE is constituted by stacking together the requested number of pillow plates. Internal welding can be made to create septa that define the flow path of the fluid inside the plates. In addition, the welding spots, and the eventual presence septa made with internal welding, define the internal path of the fluid. This enhances the flow turbulence and enlarges the area of interface between the PCM and HTF and, thus enhances heat exchange. The layout of PP-HE combines strength, solidity, simplicity and scalability [46]. The fundamental thermo-fluid dynamics characteristics of pillow plates were investigated [46,47,48] and their use in heat exchangers was considered for traditional industrial applications [49,50,51].

The main geometric specifications and operating conditions of the device analysed with CFD simulations are listed in Table 1. The specific values of the length and height of the device were defined with traditional heat exchangers with submerged plates [52] and the results of analyses previously conducted on comparable devices for on-board applications [53].

During operation, the heat transfer fluid enters the system by the inlet pipe, passes through the pillow plates and exits from the outlet pipe releasing or accumulating heat. In the charging phase, the HTF enters the system with a temperature that is sufficiently higher than that of the PCM to melt it. Thus, the former acts as the heat source and the latter as the heat sink. Conversely, in the discharge phase, the temperature of the heat transfer fluid is adequately lower than that of the storage material to solidify it through opposite actions [53]. This principle of operation allows the reserve of thermal energy to solve the mismatch between its supply and demand.

Table 1
LHS Geometrical Parameters

Parameter	Value
Inlet and outlet pipe diameter (D_e)	55 mm
Plate pipe diameter (D_p)	60 mm
Pillow Plate dimensions (W x L)	900 mm x 700 mm
Welding external diameter (D_{we})	32.64 mm
Welding internal diameter (D_{wi})	20.00 mm
Pillow Plate number (n_p)	10
Pillow plate gap (δ)	10 mm
Pillow plate gap (h_{min}, h_p)	12 mm, 15 mm
Plate thickness (t_p)	1 mm

3. Methodology

3.1. Overview of methodology: Combined CFD and reduced order modelling (ROM) for assessment of PP-LHTES

The methodology pursued in the present research combines CFD models and reduced-order models (ROM) for assessing the effects of the principal design parameters of PP-LHTES devices on their functioning in mobile applications. In particular, a multi-stage modelling approach is implemented, starting with the development of an individual modular storage unit, and examining its performance through a CFD approach. The PP-LHTES analysis is extended beyond the initial design, and a surrogate model is developed by using a systemic performance investigation across a range of scenarios, all assisted by CFD analyses. This facilitates both CFD-level analysis and the scaling of storage solutions for integration into actual vessels.

The rationale behind this methodology is to systematically develop thermal energy storage systems for mobile applications under actual conditions. By conducting the thermofluid dynamic analysis, the study advances the understanding of the dynamic operation of the storage in various operating conditions, aligning with the on-board energy system. Moreover, conducting the sensitivity analysis provides insight into key design parameters. Acknowledging that the critical parameters in storage performance lead to identifying the boundaries of technical and economic key performance indicators (KPIs), also supporting the attainment of an optimised design for individual storage units. The development of the reduced-order model evidences the practicality and flexibility of the solution. Ultimately, the scaled-up stage demonstrates the practicality and potential economic viability of the solution, offering valuable insights for decision-makers considering this technology for on-board applications.

The foundational blocks of this research are represented in Fig. 3. The assumptions and inputs considered in the CFD analysis of the modular design are supported by the literature, particularly the commercial references regarding key PP-LHTES components as the storage

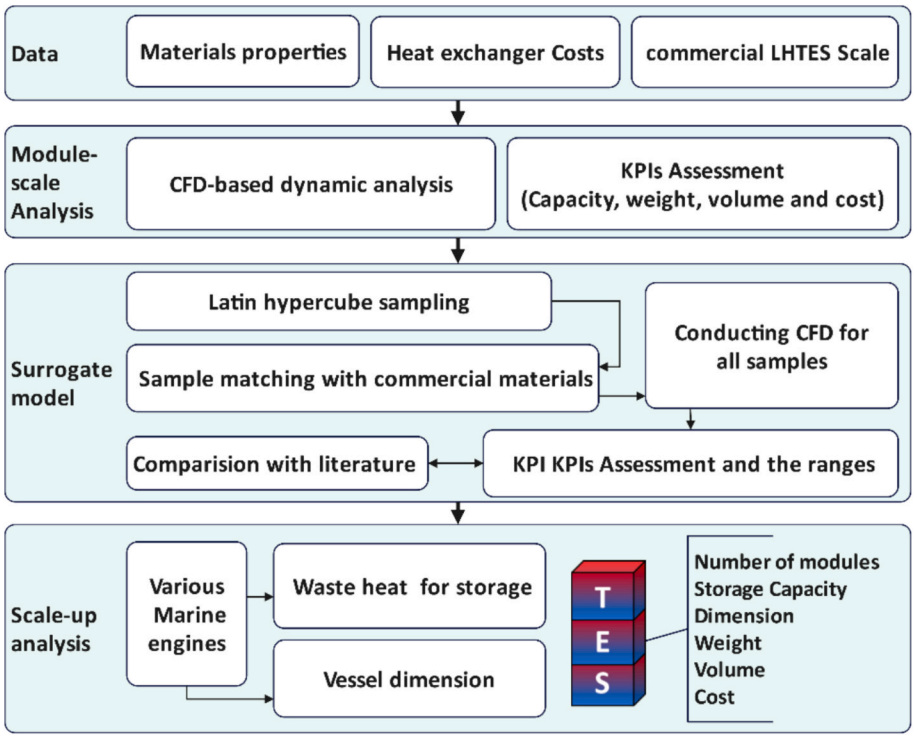

Fig. 3. Flow diagram of the PP-LHTES design approach implemented.

material and heat exchanger structure. In the following step, technical, economic, and installation KPIs are derived and extensively discussed as a complement to the CFD analysis. The surrogate model is developed upon systematic sampling with the CFD model, extending it to cover a wide range of operating conditions. The surrogate model results in a reduced-order model with detailed results, providing the opportunity for validation and comparison with the literature. In the last step, the adaptation of the solution for real-case maritime applications is discussed, and the critical challenges for on-board installation are presented.

3.2. CFD model

3.2.1. Solidification and melting model

The solidification and melting model was applied to solve the thermodynamics of the processes of phase transition of the storage material which exchanges energy with the heat transfer fluid. The model utilises an enthalpy-porosity formulation for determining the phase of the liquid–solid mushy zone of the material subject to phase change. In this context, the model includes a mushy zone constant with value within the range of $1\bullet10^5$ to $2\bullet10^5$ suggested by the literature for LHTES modelling [54]. Through this technique, the interface of phase change is not explicitly defined. Instead, the mushy zone is modelled as a porous zone with porosity equivalent to the liquid fraction, which is the ratio of the cell volume in liquid phase to the entire cell volume. The porosity of a cell ranges between 0 and 1: when the material is completely solid, the porosity is null and its velocity is zero, while, when the material is completely liquid, the porosity is unitary, and its velocity is computed. The liquid fraction is calculated for every time step by applying the enthalpy balance [55]. The momentum sink terms are also added to the momentum equations to consider the pressure drop due to the existence of the solid phase. Sink terms are even added to the turbulence equations to take into consideration the decreased porosity of the solidus [56].

Unsteady Reynolds averaged Navier-Stokes (URANS) equations were solved for an incompressible liquid. The liquid density, thermal conductivity, and dynamic viscosity were defined relying on the static value of the temperature.

The momentum equation includes a momentum sink S_{mo} arising from the reduced porosity in the mushy zone. This effect is taken into account through the source term of Eq. (1)[54,56].

$$S_{mo} = \frac{(1-\beta)^2}{(\beta^3+\varepsilon)} A_M (\boldsymbol{v} - \boldsymbol{v}_p) \tag{1}$$

where ε is a constant equal to 0.001 to prevent division by zero, A_M is the mushy zone constant, $\boldsymbol{v}$ is the liquid velocity vector, $\boldsymbol{v}_p$ is the pull velocity due to the pulling of solidified material out of the domain, and β is the liquid volume fraction defined by Eq. (2) based on the temperature of the phase change material T [56].

$$\beta = \begin{cases} 0 & T < T_{sol} \\ \dfrac{T - T_{sol}}{T_{liq} - T_{sol}} & T_{sol} < T < T_{liq} \\ 1 & T > T_{liq} \end{cases} \tag{2}$$

The mushy zone constant represents the extent of damping. As this constant increases, the velocity of the material transitions more sharply to zero as it solidifies. The pull velocity is incorporated to represent the motion of solidified material as it is steadily removed from the region during phase change [56].

The specific total enthalpy of the material H is defined as the sum of the specific sensible enthalpy h and the specific latent heat ΔH. The latent heat content is given by the product of the specific latent heat of the material L and the liquid volume fraction. The latent heat content varies from zero in the solid phase to L in the liquid phase. Consequently, Eqs. (3) and (4) are obtained [56].

$$H = h + \Delta H \tag{3}$$

$$\Delta H = \beta \mathrm{L} \tag{4}$$

The energy equation is given by Eq. (5) depending on the density ρ, the effective thermal conductivity k, the temperature T, and the source term

S_{en} [56].

$$\frac{\partial(\rho H)}{\partial t} + \nabla\cdot(\rho \mathbf{v} \mathrm{H}) = \nabla\cdot(k\nabla T + S_{en}) \quad (5)$$

The governing equations were discretised with a second-order scheme for the pressure and second-order upwind schemes for the density, momentum, and energy. The SIMPLE scheme was applied to relate velocity and pressure corrections. The least-squares, cell-based method was utilised to compute quantity gradients [56]. Flow turbulence was modelled using the laminar model with a second-order scheme, as the Reynolds number of the HTF indicates laminar behaviour [57]. The Boussinesq approximation is utilised for estimating storage material density [58,59].

The equations were implicitly solved through a pressure-based method. Also the dependency of results on the time step was explored, where the time to reach the melting temperature was examined at four different time steps: 0.1, 0.05, 0.02, and 0.01 s. The analysis showed a relative error of 1 % when comparing a case employing 0.02 to one using 0.01 s. Therefore, the value of 0.02 s was applied for transient simulation which is also aligned with the literature [41].

3.2.2. Computational domain, material and boundary conditions

Three-dimensional CFD model was employed to analyse the thermo-fluid dynamics of the flow crossing the thermal energy storage device. The computational domain was generated with SolidWorks and ANSYS SpaceClaim, its spatial discretisation was obtained with ANSYS Meshing, and ANSYS Fluent was applied for the numerical simulations. Version 21.1 of the software was utilised.

The TES system is composed of pillow plates with identical geometry, that is symmetrical relative to the longitudinal plane as illustrated in Fig. 4(a). The flow conditions of the heat transfer fluid passing through them can be approximated as equivalent for each plate owing to the manifolds acting as plenum pipes. Furthermore, the influence of the heat losses through the tank walls on the process of heat exchange between each PCM layer and the HTF inside every plate is limited due to the thermal insulation outside the tank and the relevant number of plates present. Consequently, the symmetry of the geometry and thermo-fluid dynamics conditions enables performing analyses on a computational domain comprising half of a pillow plate and the storage medium surrounding it as visible in Fig. 4(b). Thus, the computational time and resources required for the simulations are significantly diminished as it is necessary to carry out an extended sensitivity analysis and investigating a large number of configurations.

The computational domain is divided into three stationary zones: the heat transfer fluid, the pillow plate metal sheet and the phase change material. Adequate surfaces were generated at the interfaces between the HTF and metal zones and between the metal and PCM zones to solve the heat transfer process [41].

The spatial discretisation of the computational domain was achieved with either mapped or unmapped approaches. An unmapped mesh with polyhedral elements was generated for the HTF and metal zones, while a mapped mesh with hexahedral elements and an H-type topology was created for the PCM zone. The mapped grid was refined near the inlet and outlet surfaces and corresponding to the circular welding of the pillow plate.

The mesh is composed of roughly 1 million elements, whose 25 % are dedicated to the metal zone, 62 % are allocated to the PCM zone, and the remaining 13 % are assigned to the HTF. The mesh quality allows achieving solutions that fulfil the convergence criteria of the mass conservation within 10^{-3} and the maximum order of the root mean squares residuals of 10^{-6} for the continuity, momentum, energy and turbulence equations [41].

A mesh sensitivity analysis was carried out to ensure the spatial independence of computational discretisation. The outcomes of the primary fluid dynamic quantities obtained with diverse grids with a total node number ranging from 0.3 to 3.0 million were compared amongst themselves. The level of refinement of the grid was varied by proportional modifications of the element number of the three cell zones regarding the selected mesh [41].

The thermophysical properties of the heat transfer fluid and phase change materials used in the CFD analyses are listed in Table 2. The HTF is Therminol 66 for all cases, while different PCMs were considered for assessing the performance of various configurations of TES devices. The

Table 2
Thermophysical properties of HTF and PCMs utilised in the CFD simulations [61,62].

Parameter			Value
HTF (Therminol 66)	C_p [kJ/kgK]	373 K	1.84
		473 K	2.19
	Density, ρ [kg/m3]	373 K	955
		473 K	885
PCM	C_p [kJ/kgK]		1.5 … 2.3
	Thermal conductivity [W/mK]		0.36 … 0.51
	Density [kg/m^3]		900 … 1600
	Latent heat (LH) [kJ/kg]	PlusICE: H105, H115, H120	125, 100,120
		PlusICE: A82, A95,	240, 250
		PlusICE: X80, X90,120, 130	160, 170, 185,315
		Rubitherm RT: 100, 111	120, 190
	$T_{melting}$ [°C]	PlusICE: H105, H115, H120	105, 115,120
		PlusICE: A82, A95,	82, 95
		PlusICE: X80, X90,120, 130	80, 90, 120, 130
		Rubitherm RT: 100, 111	100, 111

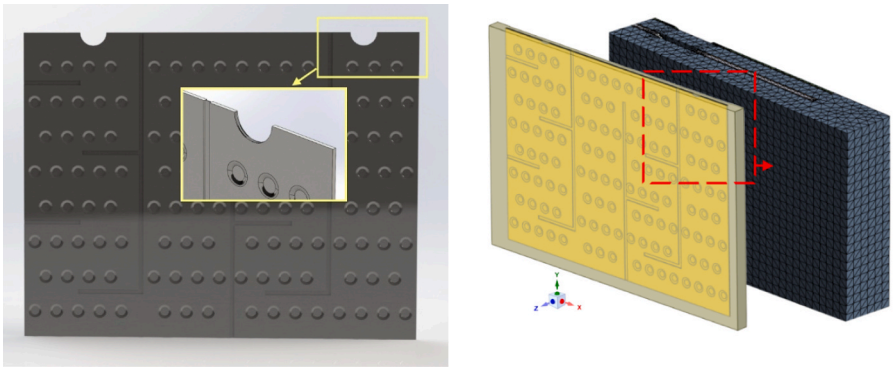

Fig. 4. Rendering of (a) one pillow plate and (b) the computational mesh of the CFD analyses for the TES device.

specific HTF was selected as it has a relatively high specific heat capacity and it provides precise temperature control for various applications The phase change material selection is of paramount importance in the design of TES systems, and it directly affects all the performance parameters such as the energy storage capacity and the charge and discharge behaviour of the unit. The set of PCMs investigated was defined to analyse a set of solutions with a melting temperature around the average between the minimum and maximum temperature values of the HTF. Amongst the selected materials, different PCMs were analysed to assess the effects of specific heat capacity, thermal conductivity, density and latent heat on thermal energy storage. The compositions of the storage materials are tailored by the supplier for different melting temperatures. However, they are mostly mixtures of nitrate salts [60].

3.3. Sensitivity analysis and reduced-order model

The objective of sensitivity analysis for the present study is to (a) quantify the impact of each parameter and (b) identify the parameters that most significantly influence simulation outcomes. Therefore, specific consideration is given to the approach of analysis both in the design of experiments as well as in the classification of improving the set of experiments to enhance the practicality of results.

Based on the literature dealing with the sensitivity of time-consuming models, the Latin Hypercube Sampling (LHS) is selected for defining sensitivity analysis CFD cases and supporting the development of the reduced-order model [63]. This method involves partitioning the search space into equal intervals along each axis, forming a hypercube to facilitate systematic variation of input parameters and alteration of multiple inputs. In the present study, LHS is used to generate 100 sets of random samples across four dimensions: HTF mass flow, PCM melting temperature, source heat temperature, and latent heat, as depicted in Fig. 5(a). LHS sampling effectively reduces the number of samples needed to achieve a desired accuracy and enhances the coverage of the parameter space with a predetermined number of samples in a multidimensional environment. Table 3 outlines the parameter ranges.

The case definition is therefore followed by one post-processing step. Each randomly generated characteristic is compared with commercially available PCMs to identify those PCMs that most closely match in terms of latent heat and phase change temperature. Through such integration, the search space comprises two discrete parameters of PCM property and two continuous parameters of operating conditions. The revised and classified cases are illustrated in Fig. 5(b) where the commercial PCMs are labelled in terms of their melting temperature and latent heat, where the first three digits stand for the melting temperature in °C and the next three for the latent heat in kJ/kg.

Table 3
Range of parameters applied to LHS of PCMs.

Property	Unit	Range
HTF Mass flow rate	kg/s	0.06… 0.8
Heat source temperature	°C	80…200
Phase change temperature	°C	82 … 133
Latent heat	kJ/kg	180…240

Following the generation of the revised set of inputs, each of them is applied to the CFD model, and the corresponding CFD results are used to discuss the (a) impact and assess the sensitivity of PP-LHTES to the input parameters.

3.4. Economic model and KPIs

The economic assessment is based on the purchase cost ($C_{P0,ref}$) calculated from the cost of components, given by Eq. (6), including heat exchanger, storage medium, and HTF. The cost of scaled storage (C_{P0}) is derived from Eq. (7) where the Chemical Engineering Plant Cost Index (CEPCI) is applied to adjust the value in time.

Exploring the heat exchanger cost curves available in the literature, the shell and tube heat exchanger (STHE) exhibits the highest similarity to the configuration used in the heat exchanger in PP-LHTES. This similarity is attributed to the PP-LHTES design, which includes a bundle of plates submerged in a container, mirroring the function of tubes in an STHE, while the container itself acts equivalently to the shell in an STHE. Given this alignment in design principles, the cost curve for the conventional STHE is identified as an appropriate benchmark for estimating the financial aspects of the PP-LHTES heat exchanger. In the present study, the STHE cost is determined as the high end of exchanger cost, and the plate heat exchanger is determined as the low bound of the cost range of the exchanger which is discussed within the sensitivity analysis.

$$C_{P0,ref} = C_{P0,PCM} + C_{P0,HE} + C_{P0,HTF} \quad (6)$$

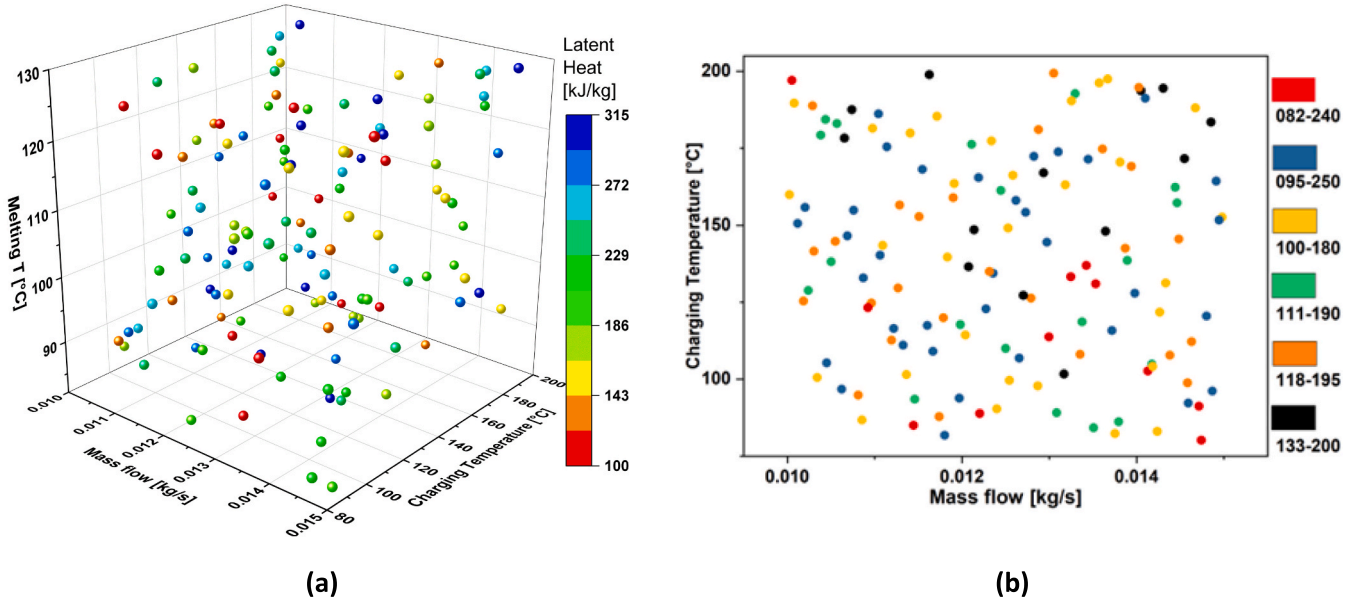

Fig. 5. Initial LHS design of experiments (a), classified data matching commercial PCMs (b).

$$C_{P0} = C_{P0,ref} \times \left[\frac{Cap_{TES}}{Cap_{ref}}\right]^{n} \times \frac{CEPCI_{2023}}{CEPCI_{ref}} \quad (7)$$

This assumption is based on the container being constructed in aluminum, equivalent to the shell in a STHE, and the plates are made of stainless steel as listed in Table 4.

For scaling up TES, the TES capacity (Cap_{TES}) can be assessed using Eq. (8), developed based on the waste heat potential ($WHR_{potnential}$) of 6 to 11.4 % [68] and the efficiency of marine engines within 40 % to 50 % [69]. To determine the intermittency in available waste heat, a ratio of standard deviation (SD) to the average value from the literature [70] is considered, which ranges from 1 to 20 % and can be used as an indicator of the intermittent waste heat available on board that can be used for charging energy storage [71]. The TES cycle time (CT), assumed to be half a day, is also a necessary consideration for TES sizing and scaling. This assumption aligns with the literature recommendation, i.e., the minimum suggested charging time of 4 h for industrial LHTES [72], and is shorter than the average journey duration of various vessels, such as 1 day for ferries or a week for cruise ships [73].

$$Cap_{TES}\,[kWh] = Cap_{ME}\,[kW] \times \frac{1-eff_{ME}}{eff_{ME}} \times \left(WHR_{potnential}[\%] \times 100\right) \times \left[\left(\frac{SD}{average}\right)_{speed}\right] \times CT_{TES}[h] \quad (8)$$

Indeed for modular TES, the number of TES systems (N_{TES}) is derived from Eq. (9) by dividing the total storage capacity by that of the TES modular unit.

$$N_{TES} = Cap_{TES}\,[kWh] / Cap_{TES,\,modular}\,[kWh] \quad (9)$$

3.5. Model validation

Before discussing the results, it is essential to validate the numerical model employed to develop the thermal performance of PP-LHTES. The model is adapted to simulate two TES case studies from the literature. The first is the study experimentally conducted by Longeon et al [74]. Indeed, the reference case study differs in configuration, but uses the same class of PCM from the same supplier as included in the main thermal analysis of the present study. In particular, RT35 supplied by Rubitherm and water were integrated in the reference study as PCM and HTF respectively. In order to maximise the value of validation, the same numerical solver details are used: time step, mushy zone parameter, and discretisation schemes. The result taken from the model is compared against the experiments, which is represented in Fig. 6, showcasing the temperature of PCM at three different distances from the surface of the heat transfer HTF pipe during the TES charging. The average of the temperature residuals, the absolute difference between model results and experiments, found to be about 0.5 °C, confirms the accuracy of the model in capturing the melting of the PCM during the charging process. The validation confirms the model for further analysis of LHTES with alternative configurations.

The second verification case study is associated with a high-temperature TES system that uses a flat plate heat exchanger with rectangular enclosures filled with PCM, which was a KNO_3-$NaNO_3$ mixture with a melting temperature of ~ 220 °C [75]. The thermal oil flows through the plates, exchanging heat with the storage materials. Two thermocouples are positioned at different horizontal distances from the plate. The reference study explored both charging and discharging processes; however, discharging is used as the reference. The experimental readings reported by Vogel et al. [75] are [20,75]used to evaluate the CFD model employed in the present study. Both the simulation results and the reference data are presented in Fig. 7, and a reasonable agreement is found for the phase change as well as the duration of discharging. The deviation in temperature is also calculated, and over 7 h of discharging, the temperature residual is found to be approximately 1.05 °C.

Table 4
Assumptions of TES economic assessment.

	Unit	Minimum	Maximum	Average	Reference
TES component: PCM	€/kg	1	10	5.5	[64,65]
TES component: exchanger	€/m^2	250	795	450	[66]
TES component: HTF	€/kg	0.4	5	2.6	[67]

4. Results and discussion

4.1. Detailed results from CFD modelling

4.1.1. Charging-discharging cycle

The dynamics of charging and discharging the PP-LHTES device are assessed by a CFD approach, providing insight into the process of energy storage and energy release in this particular TES system. It also leads to advancement in understanding the time needed to complete a full cycle of charge and discharge. The case with a melting temperature of around 89 °C was selected to evaluate the charging process. The PCM, source, and sink temperatures are represented in Fig. 8, along the charging and discharging process. As shown in Fig. 8, the charge stage firstly involves a temperature increase of the PCM from the ambient temperature of about 20 °C to the melting temperature range, and heat storage is in the form of sensible heat. Then, the energy is stored in the form of latent heat at a constant temperature. Upon receiving further heat from the heat source, the temperature of the PCM further increases beyond the melting range to a temperature close to the source temperature of 100 °C. In the zone of latent heat, the temperature remains within the bounded temperature interval of the solidification and melting temperature in Eq. (2), which is associated with the mushy zone or 2-phase condition of the storage medium. The graph represents two temperatures including the mean (M) temperature of the PCM and the temperature of a point near the HTF inlet within the PP-LHTES, denoted by NI (near inlet). The rationale behind this differentiation is to determine the difference in heat exchange during the charging and discharging process across different parts of the storage medium. As shown in Fig. 8, while both temperature observations have the same patterns during the charging and discharging cycle, a difference is found when the storage medium is in the mushy zone. This difference is associated with a) the melting and solidification of local parts within the storage medium taking less time in the vicinity of the HTF inlet, in which the temperature difference between the HTF and the PCM is at its maximum level. This results in a more effective heat exchange between the source (HTF) and the sink (PCM), thereby resulting in a faster response in temperature change and the potential phase change. As HTF flows through the PP, its temperature drops, which leads to a reduction in the HTF temperature difference thereby a delayed change in the average temperature of the storage medium. b) Despite enhanced heat distribution by the PP, there is still some non-uniformity of heat distribution, and this is pronounced more in the local zones of the storage medium with the highest distance from the heating element, like in the container corner. This fact imposes a delayed change in the average storage medium temperature which accounts for the entire storage medium.

Moreover, as shown in Fig. 8, reaching the fully charged state, observed by the average liquid fraction, is achieved within 2 h. In an ideal scenario, discharging with the same temperature difference as that of charging takes place in almost the same duration. However, this may not be practical in the actual integration of TES on board vessels. To further clarify the difference and better align with actual boundary conditions on board, independent investigations were conducted for charging and discharging.

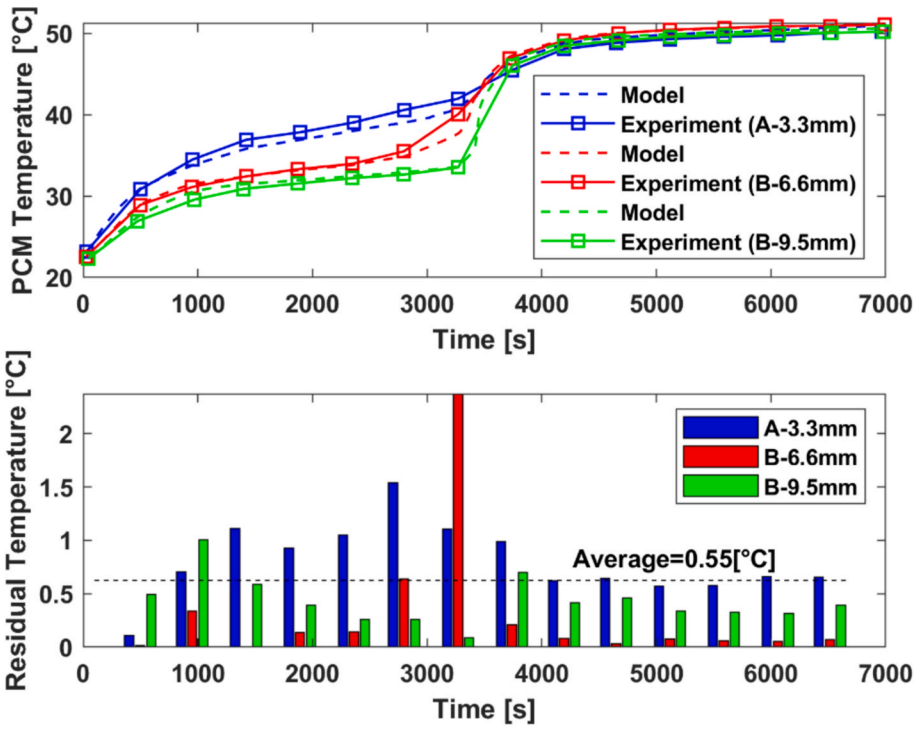

Fig. 6. Validation of the proposed LHTES CFD model through the comparison with experimental literature data (low temperature).

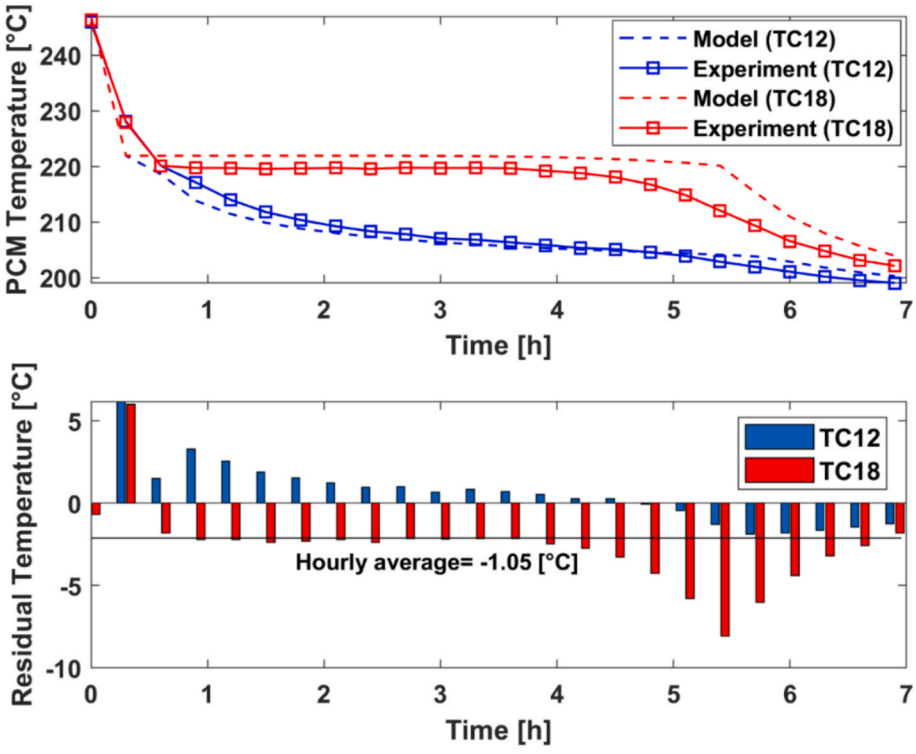

Fig. 7. Validation of the proposed LHTES CFD model through the comparison with experimental literature data (High temperature).

4.1.2. PP-LHTES charging process

The effect of source condition on the charging process was explored by considering different temperatures and integrating the same PCM as Section 4.1.1, in the PP-LHTES. As shown in Fig. 9, a higher source temperature results in a shorter charging time, due to a greater temperature difference, which facilitates the heat exchange between HTF and PCM. Using a source temperature of 170 °C results in a quicker charging process, cutting the time by 50 % compared to the case with melting temperature of 120 °C. It is worth noting that utilising alternative source temperatures does not alter the latent heat storage capability but increases the storage in the form of sensible heat. Although the storage capacity of the PP-LHTES device is predominantly based on

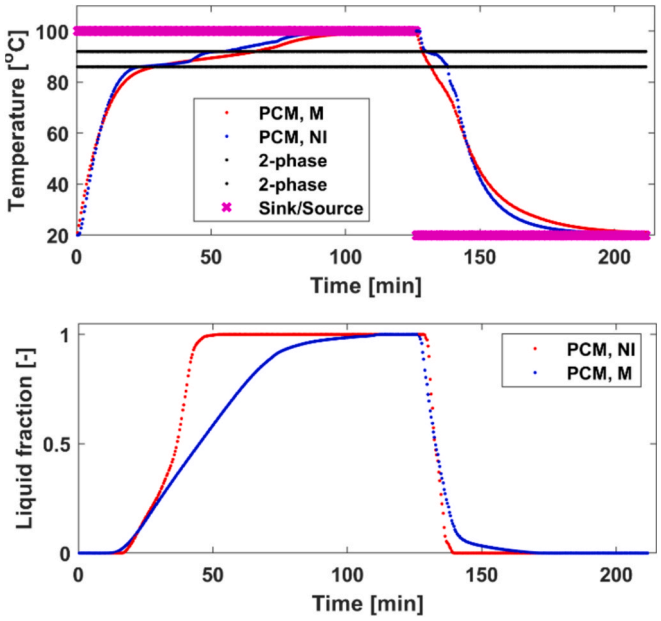

Fig. 8. Variation in discharging duration for different sink temperatures (Legend: NI – Near Inlet; M – Mean).

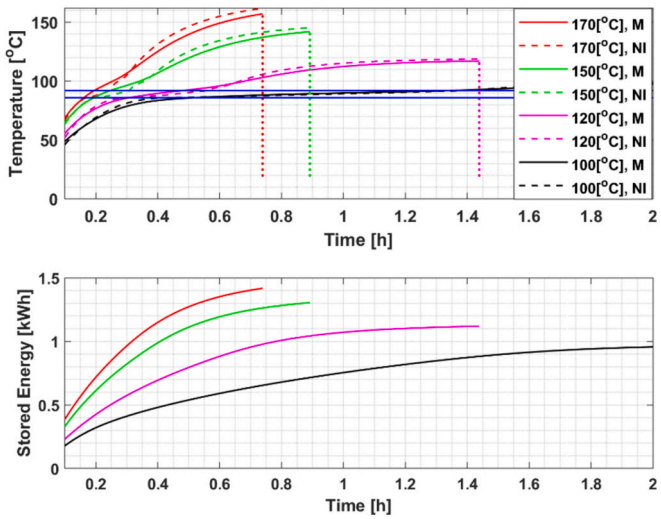

Fig. 9. Variation in charging time and storage capacity under different conditions (Blue lines represent Liquidus and Solidus Temperatures). (For interpretation of the references to colour in this figure legend, the reader is referred to the web version of this article.)

latent heat, increasing the source temperature boosts the contribution of sensible heat. This heat storage capacity improvement is estimated at 50 % of the overall storage capacity, which is depicted in Fig. 9 for a single pillow plate when the source temperature is increased from 100 °C to 170 °C. However, the source temperature condition is usually imposed by the waste heat source condition on board, and TES design parameters, including the type of PCM and the associated melting temperature, should be selected properly to maximise the PP-LHTES integration and performance.

Fig. 10 complements the previous investigation by focusing on the role of the HTF's mass flow rate. The examination is based on the same operating conditions as **Section 4.1.1**, including the charging temperature and the type of PCM. Utilising an HTF with a higher mass flow rate contributes to maintaining a lower temperature drop in the HTF when it passes through the pillow plates (PPs), facilitating a more uniform heat exchange between the heating elements (PPs) and the storage medium. However, the results shown in Fig. 10 also evidence the negligible impact of mass flow rate change on the PP-LHTES charging time. A higher mass flow rate requires more power for the circulation of HTF through the pillow plates; therefore, considering the trade-off between the increased power needed for a higher mass flow rate and the slight reduction in the TES charging time, along with observing no impact on the storage capacity, an increase in the mass flow rate is not a beneficial option.

The other critical parameter in PP-LHTES design is the type of storage material. A wide range of PCMs, listed in Table 2, with different thermophysical properties were evaluated to explore the charging process under a fixed source temperature. Such investigation provides a guideline for selecting the PCMs according to the energy storage requirements on board vessels. The detailed results in charging time particularly support tailoring the PP-LHTES design to be responsive in time and properly scaled for capturing on-board WH. Different PCMs commercially available in the market were evaluated [61], considering organic PCMs (A-type), solid–solid (X-type), and inorganic ones (H-type). As shown in Fig. 11, organic PCMs have a shorter charging time than the other classes of storage medium. Further investigation by discussing the PCM thermophysical properties is provided in the sensitivity analysis in **Section 4.2.1**.

4.1.3. PP-LHTES discharging process

Independent analysis is conducted for the PP-LHTES discharging process. The temperature difference utilised for discharging evaluation is differently adjusted compared to that of the charging process, aligning more with the practical integration of TES charging. The energy released from the TES is potentially used in fulfilling on-board heat demand or supporting another WHR. According to the references, the temperature for heat demand, like for hot water demand, is a minimum of 50 °C [49]. Moreover, the minimum temperature that ORC, as the most distinguished WHR technology, is reported at 50 °C for the recovery of low-grade heat for maritime applications [24]. Therefore, a range of sink temperatures starting from 50 °C are considered for PP-LHTES discharging. Obviously, the associated temperature difference between the temperature of the storage medium at the charged state and the sink is less than that in the charging stage. As shown in Fig. 12, the TES full discharging takes between 4 and 6 h, which is substantially longer than the charging time because of the lower heat transfer rate during discharge, echoed in the literature for LTHTES devices [76]. The PP-LHTES charging to discharging time ratio is estimated within 1.3 to 2.5, which is in agreement with the literature for LHTES systems [77].

4.2. Sensitivity analysis results and reduced-order model

4.2.1. CFD-base parametric analysis of TES performance

The sensitivity analysis conducted as part of this study aimed to quantify the impact of various parameters on the performance of PCM systems. As shown in Fig. 13a, the influence of HTF mass flow on the charging process of the system. The HTF mass flow was identified as having a marginal impact. This observation is consistent with the findings of Shen et al. [78] and Kabbara et al. [79], who reported that the effect of HTF on the time required to reach a fully charged state is negligible. Furthermore, the overall heat transfer efficiency is predominantly influenced by the PCM properties rather than the HTF dynamics. The two PCM characteristics show a relevant impact on the storage charging time. According to the sensitivity analysis results, as shown in Fig. 13b, embedding a PCM with a higher melting point results in a 20 % longer charging time under identical operating conditions of the heat sink. This finding is consistent with the research of Marri et al. reporting an increase of up to 50 % in charging time when utilising a PCM under the same operating conditions of the heat sink [80].

The impact of latent heat is demonstrated in Fig. 13c which is found to be more significant, increasing charging time by 15 % for a PCM with

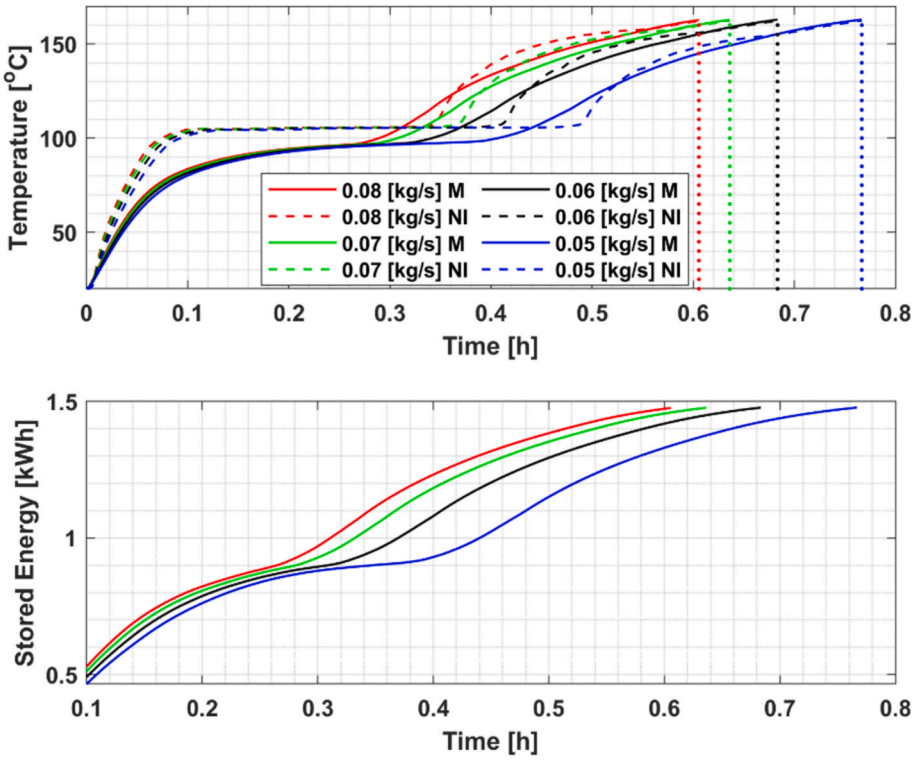

Fig. 10. Variation in charging time and storage capacity for different mass flow rates of the HTF (Legend: NI – Near Inlet; M – Mean).

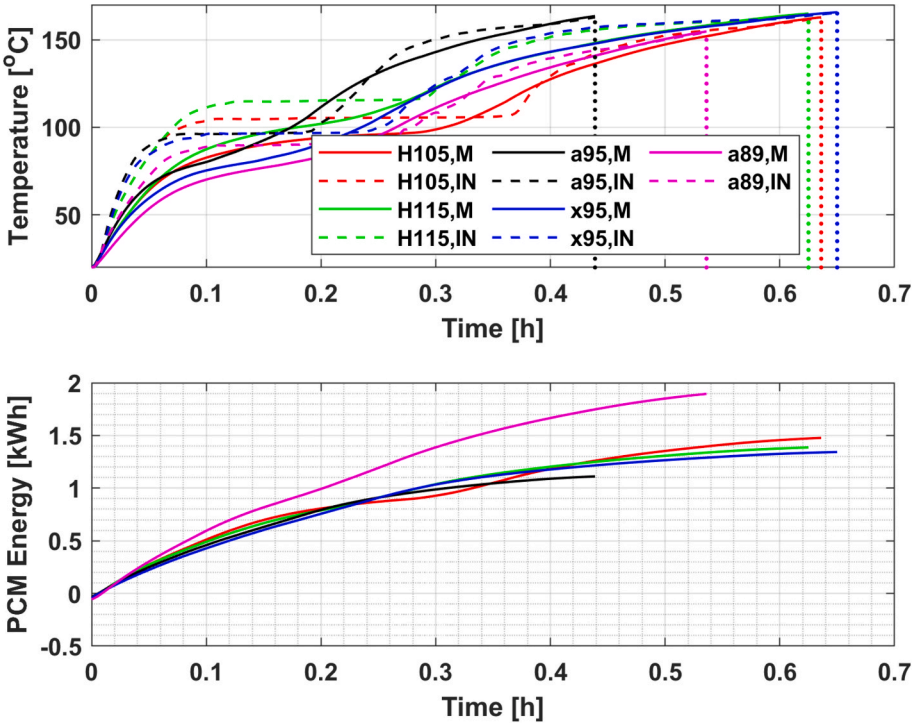

Fig. 11. Variation in charging time for different phase change materials (Legend: NI – Near Inlet; M – Mean).

double the latent heat value. This conclusion is drawn by comparing the averages of two clusters specified in Fig. 13**c.** The rationale behind this impact is the delay in heat exchange during the phase change that occurs during the charging process. This observation aligns with the literature, including the study by Narasimhan et al., which discovered that a 35 % increase in the latent heat of the first PCM delays the melting process by 9 % [81]. The results presented in Fig. 13 show a lack of linear correlation between the parameters. A statistical analysis with linear fitting is also conducted to support this conclusion. The goodness of fit is determined by considering the residuals between the CFD model result (y) and the predicted values by the linear regression ($\hat{y}$). The Root mean squared error (RMSE), defined as Eq. (10), for charging time shown in

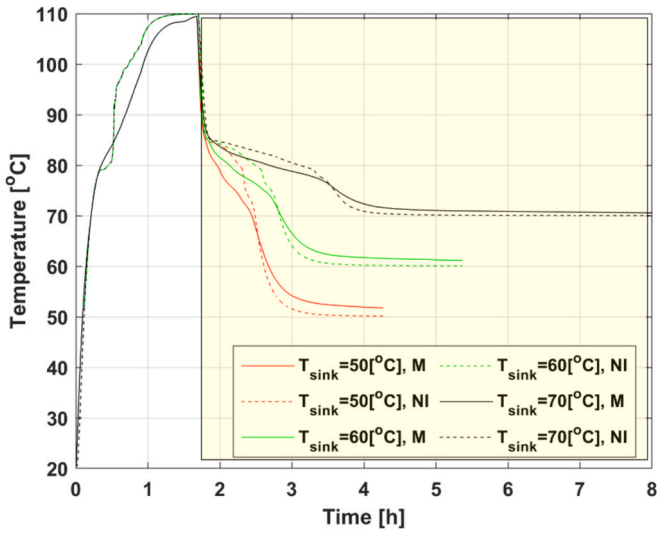

Fig. 12. Variation in discharging time for different sink temperatures (Legend: NI – Near Inlet; M – Mean).

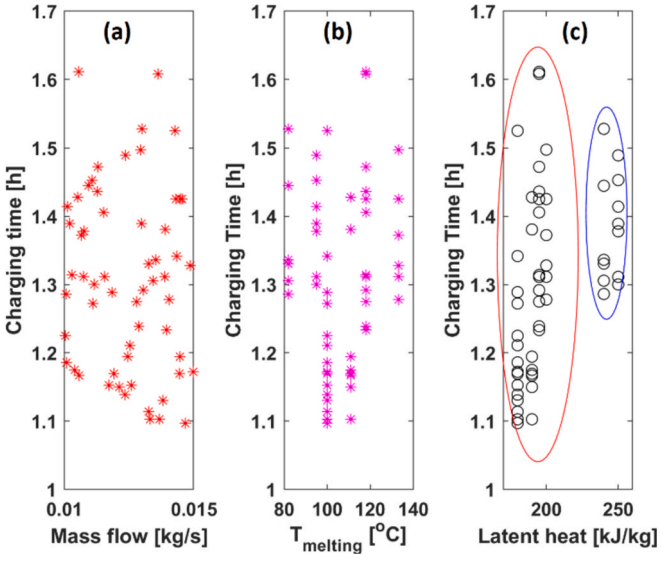

Fig. 13. CFD-based sensitivity analysis.

Fig. 13a–c are found as 0.133, 0.132, and 0.120, with R-squared all less than 0.2, reflecting the lack of linear correlation between those parameters.

$$\mathrm{RMSE} = \sqrt{\frac{1}{n}\sum_{i=1}^{n}(y_i - \hat{y}_i)^2} \tag{10}$$

Fig. 14 complements the results shown in Fig. 13, representing the classification commercial PCMs from multiple PCM suppliers used in the sensitivity analysis [61,62]. Different PCMs from various suppliers may have differences in chemical composition and physical properties; however, an almost linear decrease is found for the charging time of the of the PP-LHTES in the present study, with capacity within the range of 17 kWh to 22 kWh. Considering the confidence margin, a simple regression can be used to extrapolate the charging time based on the source temperature. The associated RMSE, found to be 0.115, is less than all fitted equations for previous variables, which represent a better fit. Thereby, it is demonstrated separately to explore the linearity. The result provided in Fig. 14 can be utilised as a reference for PCM selection from the commercial PCMs. It can also serve as a rule of thumb for

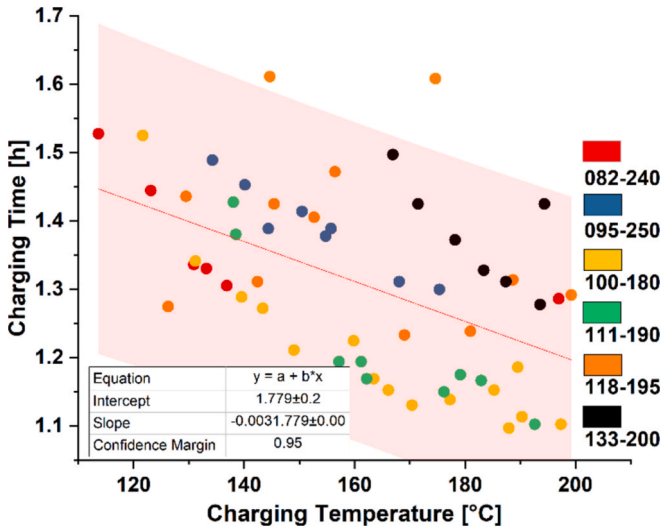

Fig. 14. Sensitivity analysis obtained with the CFD simulations. (legend format: T-LH; T is the melting temperature in °C and the LH is the latent heat in kJ/kg).

charging time estimation for a known charging temperature. It is quite common that the TES operating temperature and the charging-discharging cycle are imposed by the source and sink conditions; therefore a proper PCM selection in LHTES design is essential to match the timing—i.e., looking at Fig. 14 for a PCM for integration into a PP-LHTES with a mid-range charging time of 1.4 h and mid-range charging temperature of 140 °C, there are multiple PCMs with different melting temperature and latent heat values which can be used interchangeably.

4.2.2. Economic assessment of the LHTES and on-board installations KPIs

Although the scale and size of the results from CFD presented in Section 4.1 are determined as an educated guess, supported by evidence in the literature for a single modular energy storage unit, there remain some uncertainties associated with the design and cost assumptions. Consequently, a detailed sensitivity analysis is conducted to assess the energy storage capacity of a single unit and its purchase cost. A ± 20 % change is applied to six technical parameters as well as to the cost units of PP-LHTES components. The impact of variation in each on both storage capacity and purchase cost of TES is assessed, while the remaining parameters are kept unchanged. The results, depicted in Fig. 15, provide insights into both individual and combined effects of

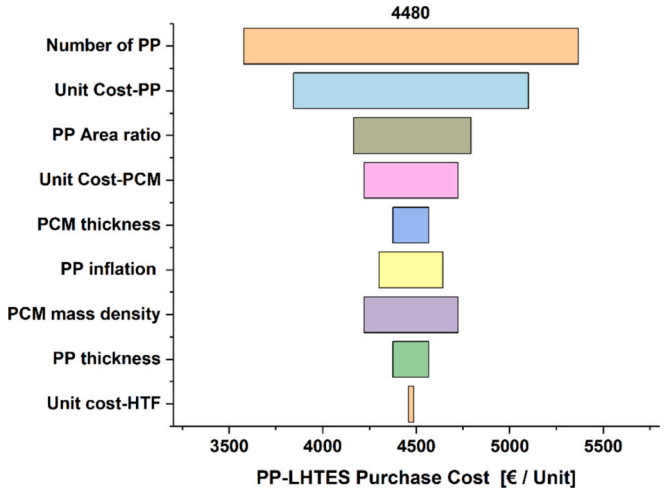

Fig. 15. Purchase cost of PP-LHTES unit.

these variations, offering a comprehensive overview of the individual PP-LHTES module. As illustrated, among technical items, the impact of PP numbers is the most significant, followed by the unit cost of the PP area ratio. Having a rough estimation of the cost of PP-LHTES at about 4500€ per module can be used as a reference for calculating the expenses involved in scaling up the storage solution for vessels.

Installing new technology on board vessels requires careful consideration regarding the spatial and weight constraints in the engine room [82]. In this context, Fig. 16 complements Fig. 15 with further KPIs for on-board installation, including weight, volume, and energy capacity, along with the cost of a storage module comprising 10 pillow plates. The weight and volume of PP-LHTES module are shown in Fig. 16. However, to better address compactness, the weight and volume of PP-LHTES is compared with the weight and size of standard on-board equipment. The weight of Wärtsilä marine engines is considered as a baseline which is reported from 9 to 200 t, occupying up to 380 m^3 [83]. In comparison, an individual PP-LHTES module weighs 0.5 t and occupies a 0.25 m^3, which does not impose a critical challenge to fit PP-LHTES within the engine room(see Fig. 17).

In order to evaluate the advantages of the proposed PP + LHTES, the KPIs are validated against existing literature, mainly those that are commercialised and available in the market. The average purchase cost of a PP-LHTES module reaches 206 €/kWh, which is lower than LHTES systems available in the market including LHTES system by Sunamp with average specific storage cost of 241 €/kWh. Moreover, the volumetric energy density is much higher than the LHTES in the literature, 89 against 53 kWh/m3. Its specific energy density is also competitive, falling within the range of 45 to 50 kWh/t, which is similar to the values reported in the literature. All these three KPIs, evidence PP-LHTES as a more compact and cost-effective storage solution.

4.2.3. PP-LHTES scale-up

Upon validating the KPIs and particularly the storage capacity with the average found to be 22kWh (See Fig. 16), it becomes possible to accurately assess the number of TES units that can be accommodated within the energy systems of vessels of various sizes, as well as the weight and volume of the scaled TES. This enables a practical discussion on the feasibility of integrating TES, taking into account the spatial constraints inherent in vessels. Marine engines produced by Wärtsilä are considered as the representative component of vessel scale; therefore, the total capacity of TES is estimated based on the available intermittent waste heat. The number of PP-LHTES is then calculated using the individual module capacity. As shown in Fig. 18, the number of required modules lies within 2 to 60, depending on the vessel scale, and the total weight and volume reach 30 t and 16 m^3 for a vessel with a ME of 18 MW, respectively. Relatively, these estimates equate to only 15 % and 5 % of the mass and volume of marine engines, indicating a relatively small addition in terms of overall weight and space occupied. This estimation aligns with literature on WHR technology integration by Pallis et al. that investigated modular ORC on board with a 3D model within the vessel engine room [88]. Therefore, integrating a TES system on board a vessel has a minimal spatial footprint, comparable to other WHR technologies, and is manageable in vessel design for new vessels or retrofitting an existing vessel. Moreover, the weight of the TES system can be compared to the weight of a loaded standard twenty-foot container (TEU) with a weight within 9 to 24 t [89,90]. Referring to the literature, loading an extra TEU on board incurs about a 0.003 % increase in fuel consumption of midrange vessels [91]. It is also reported within 0.0002 % to 0.0003 % per extra tonne of DWT [92,93]. Upon

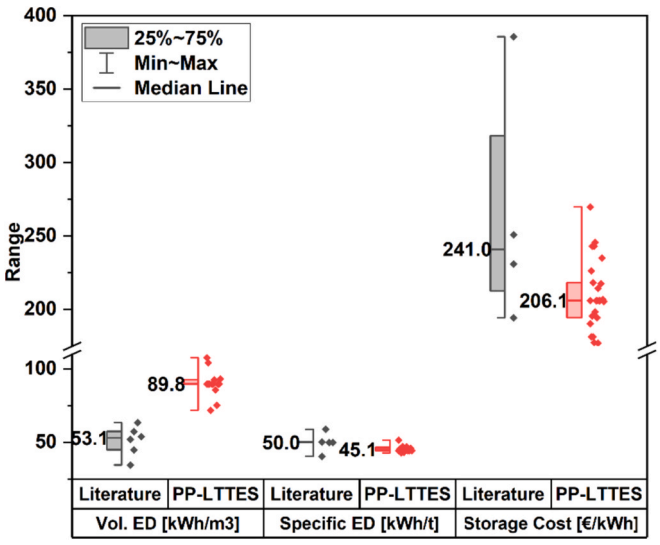

Fig. 17. Energy storage characteristics validation against literature (ED: energy density) obtained based on literature data [84,85,86,87].

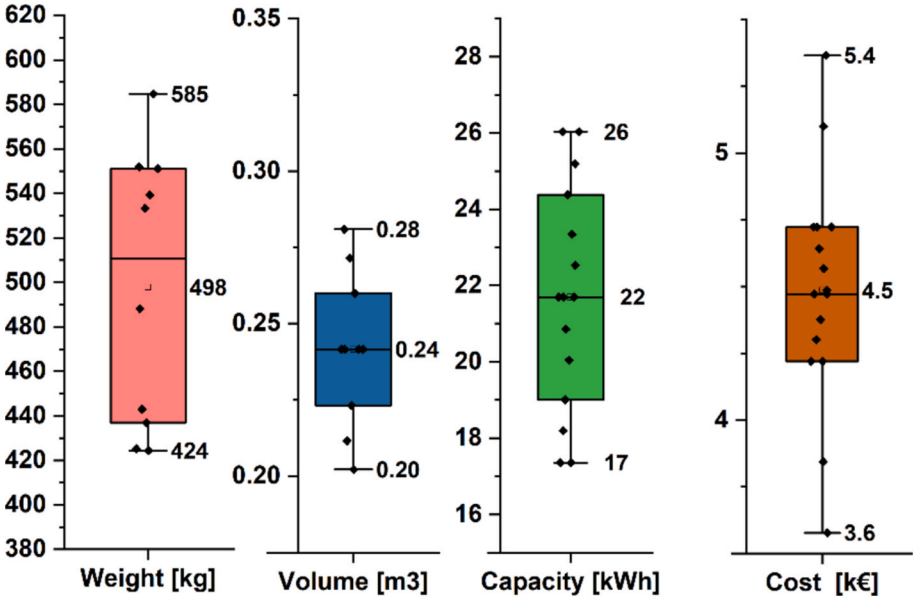

Fig. 16. Sensitivity analysis of the main design parameters of TES systems obtained with CFD simulations.

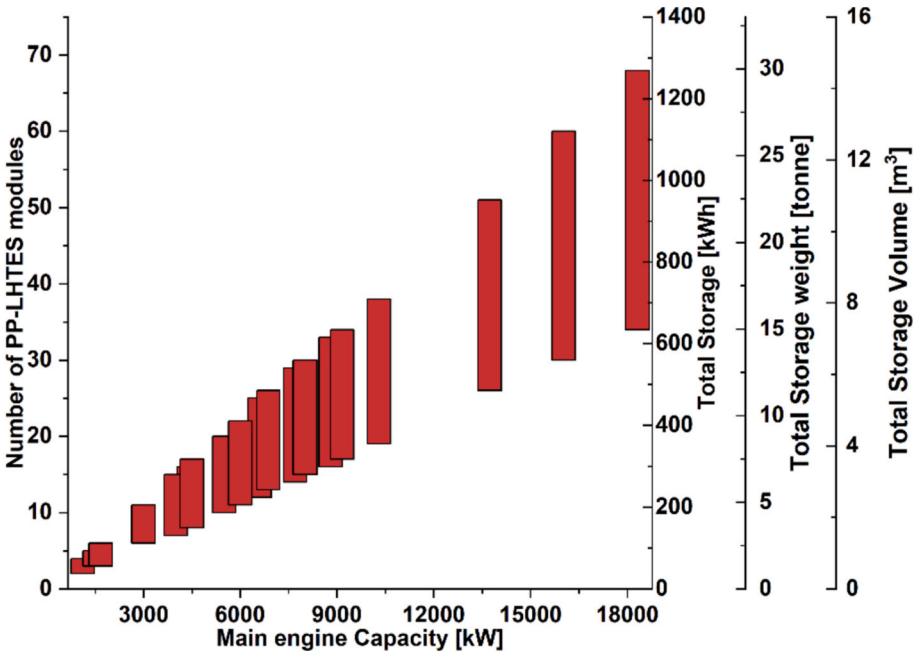

Fig. 18. TES load on board different vessels.

these rule-of-thumb calculations, thereby the additional fuel consumption incurred by loading a mid-scale PP-LHTES on board is estimated as negligible as 0.003 %. Considering a mid-range cargo vessel with a capacity of 2000 TEU with an average 12 MW ME capacity may require, the weight of mid-range PP-LHTES accounts for 12 t equivalent to about 1 TEU equivalent to about 0.05 % of TEU capacity.

Moreover, the cost of scaled-up TES is compared to the capital cost of vessels, estimated by dividing the commercial value of the fleet in a vessel class [94] by the number of vessels [95], which is found to be 70 million euro for container cargo and 240 million euro for cruise ships. It is found that the TES cost ranges from 0.2 % of the capital cost of the vessel, which appears affordable for ship owners.

5. Conclusions

The present investigation thoroughly examined the technical and economic performance of a modular LHTES device that uses pillow plate heat exchangers incorporating phase change materials (PCMs) for a novel application in waste heat recovery (WHR) on board vessels. Through a comprehensive techno-economic analysis, the investigation enhances the understanding of PP-LHTES performance. The technical discussion is reinforced by a systematic analysis using CFD methods to deepen insights into storage performance beyond existing literature. Additionally, there is an in-depth exploration of the storage capacity of PP-LHTES systems and the optimal selection of storage materials. The study is further enriched by a detailed economic analysis, which examines scaled-up versions of the storage solution designed to accommodate various vessel sizes.

The key findings of the present research are listed in the following:

- The full cycle of PP-LHTES charging and discharging is found within 2–3 h, aligning with the intermittent nature of waste heat on board vessels.
- The specific energy density of PP-LHTES is found in agreement with that of LHTES in the literature; however, the volumetric energy density of PP-LHTES is found to be up to 1.8 times that of the conventional one, indicating the compactness favourable for on-board integration.
- It was revealed by detailed scaling-up investigation that the incurred impact of integrating PP-LHTES in terms of additional weight, volume, and the associated fuel consumption compared with the baselines of the vessel itself are negligible, all estimated at less than 0.05 %. Also, the cost of PP-LHTES is found to be less than 0.2 % of the vessel value.
- The sensitivity analysis on storage material characteristics and the boundary conditions revealed that the type of charging temperature and the PCM latent heat are the most impactful parameters. The mass flow rate of the HTF has an impact on the duration of charge and discharge even if it is lower regarding the other two parameters.
- The economic analysis on the cost of the PP-LHTES module leads to the identification of the number of PPs, the unit cost of PP, the unit cost of PCMs, and the PCM thickness as the most impactful parameters on the overall purchase cost of storage.
- The principal metrics for on-board installation including weight, spatial footprint, and energy storage capacity are determined for the PP-LHTES module. The results revealed the scalability feature of PP-LHTES, having an average weight of 500 kg and a quarter of a cubic meter volume, with an average storage capacity of 17 kWh to 22 kWh. The storage scale-up is conducted for a wide range of vessel scales in the global fleet, demonstrating the adaptability of the TES system to different vessel sizes. Scaled-up PP-LHTES are demonstrated by comparing their spatial footprint and weight with the main engine volume and weight. The results fully evidenced the solution's affordability for installation in engine rooms either for new vessels or for retrofitting existing vessels.
- The cost and benefits of PP-LHTES are evaluated by comparing the economic KPIs. It is found that PP-LHTES has the potential to be among the favourable solutions. The specific cost of storage is found at about 206 €/kWh, which is almost 10 % lower than the average specific cost of storage of available LHTES in the market. The purchase cost of PP-LHTES represents an affordable solution, costing about 0.1 % of the capital cost of an average vessel.

This research explored the technical and economic viability of the PP-LHTES system, highlighting the scale-up and sizing for involvement in advancing maritime waste heat recovery technologies.

Declaration of competing interest

The authors declare that they have no known competing financial interests or personal relationships that could have appeared to influence the work reported in this paper.

Acknowledgments

This work was supported by the Horizon Europe research and innovation programme (ZHENIT Project with grant number 101056801) and by the United Kingdom Research and Innovation (reference number 10038861).

Data availability

Data will be made available on request.

References

[1] M. Wu, K.X. Li, Y. Xiao, K.F. Yuen, Carbon emission trading scheme in the shipping sector: Drivers, challenges, and impacts, Mar. Policy 138 (2022), https://doi.org/10.1016/j.marpol.2022.104989.
[2] G. Mallouppas, E.A. Yfantis, Decarbonization in shipping industry: A review of research, technology development, and innovation proposals, J. Mar. Sci. Eng. 9 (2021), https://doi.org/10.3390/jmse9040415.
[3] D.V. Singh, E. Pedersen, A review of waste heat recovery technologies for maritime applications, Energy Convers Manag 111 (2016) 315–328, https://doi.org/10.1016/j.enconman.2015.12.073.
[4] M.A.N.D.& Turbo, Waste Heat Recovery System (WHRS), 2014.
[5] G. Shu, Y. Liang, H. Wei, H. Tian, J. Zhao, L. Liu, A review of waste heat recovery on two-stroke IC engine aboard ships, Renew. Sustain. Energy Rev. 19 (2013) 385–401, https://doi.org/10.1016/j.rser.2012.11.034.
[6] V. Palomba, G.E. Dino, R. Ghirlando, C. Micallef, A. Frazzica, Decarbonising the shipping sector: A critical analysis on the application of waste heat for refrigeration in fishing vessels, Appl. Sciences (switzerland) 9 (2019), https://doi.org/10.3390/app9235143.
[7] X. Xu, Y. Li, S.Y. Yang, G. Chen, A review of fishing vessel refrigeration systems driven by exhaust heat from engines, Appl. Energy 203 (2017) 657–676, https://doi.org/10.1016/j.apenergy.2017.06.019.
[8] J. Vinje Kramer, S. Steen, Sail-induced resistance on a wind-powered cargo ship, Ocean Engineering 261 (2022), https://doi.org/10.1016/j.oceaneng.2022.111688.
[9] Glomeep, Waste heat recovery systems , (2023). https://glomeep.imo.org/technology-groups/ (accessed March 11, 2024).
[10] S. Zhu, K. Zhang, K. Deng, A review of waste heat recovery from the marine engine with highly efficient bottoming power cycles, Renew. Sustain. Energy Rev. 120 (2020) 109611, https://doi.org/10.1016/j.rser.2019.109611.
[11] M.E. Mondejar, J.G. Andreasen, L. Pierobon, U. Larsen, M. Thern, F. Haglind, A review of the use of organic rankine cycle power systems for maritime applications, Renew. Sustain. Energy Rev. 91 (2018) 126–151, https://doi.org/10.1016/j.rser.2018.03.074.
[12] O. Konur, O. Yuksel, S.A. Korkmaz, C.O. Colpan, O.Y. Saatcioglu, I. Muslu, Thermal design and analysis of an organic rankine cycle system utilizing the main engine and cargo oil pump turbine based waste heats in a large tanker ship, J. Clean. Prod. 368 (2022), https://doi.org/10.1016/j.jclepro.2022.133230.
[13] R. Pili, A. Romagnoli, H. Spliethoff, C. Wieland, Techno-economic analysis of waste heat recovery with ORC from fluctuating industrial sources, in: Energy Procedia, Elsevier Ltd, 2017, pp. 503–510, https://doi.org/10.1016/j.egypro.2017.09.170.
[14] S. Roosjen, M. Glushenkov, A. Kronberg, S. Kersten, Waste heat recovery systems with isobaric expansion technology using pure and mixed working fluids, (2022) 1–14. https://doi.org/10.20944/preprints202207.0002.v1.
[15] K. Sztekler, W. Kalawa, W. Nowak, L. Mika, S. Gradziel, J. Krzywanski, E. Radomska, Experimental study of three-bed adsorption chiller with desalination function, Energies (basel) 13 (2020) 1–13, https://doi.org/10.3390/en13215827.
[16] B. Zalba, J.M. Marin, L.F. Cabeza, H. Mehling, Review on thermal energy storage with phase change: materials, heat transfer analysis and applications, 2003.
[17] G. Alva, Y. Lin, G. Fang, An overview of thermal energy storage systems, Energy 144 (2018) 341–378, https://doi.org/10.1016/j.energy.2017.12.037.
[18] Ó. García-Afonso, A.M. Delgado-Torres, B. González-Díaz, Potential of Organic Rankine Cycle for waste heat recovery from piston engine-based power plants in isolated power systems, Appl. Therm. Eng. 203 (2022), https://doi.org/10.1016/j.applthermaleng.2021.117815.
[19] L. Miró, J. Gasia, L.F. Cabeza, Thermal energy storage (TES) for industrial waste heat (IWH) recovery: A review, Appl. Energy 179 (2016) 284–301, https://doi.org/10.1016/j.apenergy.2016.06.147.
[20] J. Vogel, M. Johnson, Natural convection during melting in vertical finned tube latent thermal energy storage systems, Appl. Energy 246 (2019) 38–52, https://doi.org/10.1016/j.apenergy.2019.04.011.
[21] J. Vogel, M. Keller, M. Johnson, Numerical modeling of large-scale finned tube latent thermal energy storage systems, J. Energy Storage 29 (2020), https://doi.org/10.1016/j.est.2020.101389.
[22] W.-D. Steinmann, Thermal energy storage for medium and high temperatures, 1st ed.,, Springer Wiesbaden, 2021.
[23] A. Frazzica, M. Manzan, V. Palomba, V. Brancato, A. Freni, A. Pezzi, B.M. Vaglieco, Experimental validation and numerical simulation of a hybrid sensible-latent thermal energy storage for hot water provision on ships, Energies (basel) 15 (2022), https://doi.org/10.3390/en15072596.
[24] F. Catapano, A. Frazzica, A. Freni, M. Manzan, D. Micheli, V. Palomba, P. Sementa, B.M. Vaglieco, Development and experimental testing of an integrated prototype based on Stirling, ORC and a latent thermal energy storage system for waste heat recovery in naval application, Appl. Energy 311 (2022), https://doi.org/10.1016/j.apenergy.2022.118673.
[25] L. Godiff, An analytical model characterising a latent heat thermal energy storage tank, n.d.
[26] W.-B. Ye, M. Arıcı, False diffusion, asymmetrical interface, and equilibrious state for pure solid-gallium phase change modeling by enthalpy-porosity methodology, Int. Commun. Heat Mass Transfer 144 (2023) 106746, https://doi.org/10.1016/j.icheatmasstransfer.2023.106746.
[27] W.-B. Ye, M. Arıcı, 3D validation, 2D feasibility, corrected and developed correlations for pure solid-gallium phase change modeling by enthalpy-porosity methodology, Int. Commun. Heat Mass Transfer 144 (2023) 106780, https://doi.org/10.1016/j.icheatmasstransfer.2023.106780.
[28] W.-B. Ye, M. Arıcı, Exploring mushy zone constant in enthalpy-porosity methodology for accurate modeling convection-diffusion solid-liquid phase change of calcium chloride hexahydrate, Int. Commun. Heat Mass Transfer 152 (2024) 107294, https://doi.org/10.1016/j.icheatmasstransfer.2024.107294.
[29] S. Liu, Y. Li, Y. Zhang, Mathematical solutions and numerical models employed for the investigations of PCMs' phase transformations, Renew. Sustain. Energy Rev. 33 (2014) 659–674, https://doi.org/10.1016/j.rser.2014.02.032.
[30] C. Ding, Z. Niu, B. Li, D. Hong, Z. Zhang, M. Yu, Analytical modeling and thermal performance analysis of a flat plate latent heat storage unit, Appl Therm Eng 179 (2020), https://doi.org/10.1016/j.applthermaleng.2020.115722.
[31] G. Manente, Y. Ding, A. Sciacovelli, A structured procedure for the selection of thermal energy storage options for utilization and conversion of industrial waste heat, J. Energy Storage 51 (2022) 104411, https://doi.org/10.1016/j.est.2022.104411.
[32] A. Sciacovelli, E. Guelpa, V. Verda, Second law optimization of a PCM based latent heat thermal energy storage system with tree shaped fins, Int. J. Thermodyn. 17 (2014) 127–136, https://doi.org/10.5541/ijot.549.
[33] A. Pizzolato, A. Sharma, R. Ge, K. Maute, V. Verda, A. Sciacovelli, Maximization of performance in multi-tube latent heat storage – Optimization of fins topology, effect of materials selection and flow arrangements, Energy 203 (2020), https://doi.org/10.1016/j.energy.2019.02.155.
[34] I.A. Laasri, Z. Elmaazouzi, A. Outzourhit, M.O. Mghazli, Investigation of different topology-optimized fin structures in a cylindrical latent heat thermal energy storage unit, Therm. Sci. Eng. Prog. 33 (2022), https://doi.org/10.1016/j.tsep.2022.101372.
[35] R. Ge, G. Humbert, R. Martinez, M.M. Attallah, A. Sciacovelli, Additive manufacturing of a topology-optimised multi-tube energy storage device: Experimental tests and numerical analysis, Appl. Therm. Eng. 180 (2020), https://doi.org/10.1016/j.applthermaleng.2020.115878.
[36] S. Tiari, A. Hockins, K. Shank, Experimental study of a latent heat thermal energy storage system assisted by varying annular fins, J. Energy Storage 55 (2022), https://doi.org/10.1016/j.est.2022.105603.
[37] P. Royo, M. Johnson, N. David, M. Fiss, A.M. López-Sabirón, G.A. Ferreira, A. Gutierrez, Experimental analysis of a power-to-heat storage with high-temperature phase change materials to increase flexibility and sector coupling, Appl. Therm. Eng 236 (2024), https://doi.org/10.1016/j.applthermaleng.2023.121889.
[38] W. Lin, W. Zhang, Z. Ling, X. Fang, Z. Zhang, Experimental study of the thermal performance of a novel plate type heat exchanger with phase change material, Appl. Therm. Eng 178 (2020), https://doi.org/10.1016/j.applthermaleng.2020.115630.
[39] O. Galteland, M. Gouis, J. Salgado-Beceiro, A. Sevault, Fourteen months operation of a 200 kWh latent heat storage pilot, n.d.
[40] M. Mastani Joybari, H. Selvnes, E. Vingelsgård, A. Sevault, A. Hafner, Parametric study of low-temperature thermal energy storage using carbon dioxide as the phase change material in pillow plate heat exchangers, Appl. Therm. Eng 221 (2023), https://doi.org/10.1016/j.applthermaleng.2022.119796.
[41] P. Niknam, L. Ciappi, R. Fisher, A. Sciacovelli, Development of a latent heat thermal energy storage system for waste heat recovery on ships, 2023.
[42] M. Grljušic, V. Medica, G. Radica, Calculation of efficiencies of a ship power plant operating with waste heat recovery through combined heat and power production, Energies (basel) 8 (2015) 4273–4299, https://doi.org/10.3390/en8054273.
[43] P. Marty, J.F. Hétet, D. Chalet, P. Corrignan, Exergy analysis of complex ship energy systems, Entropy 18 (2016), https://doi.org/10.3390/e18040127.
[44] A.G. Mohammed, M. Mosleh, W.M. El-Maghlany, N.R. Ammar, Performance analysis of supercritical ORC utilizing marine diesel engine waste heat recovery, Alex. Eng. J. 59 (2020) 893–904, https://doi.org/10.1016/j.aej.2020.03.021.
[45] M. Saha, O. Tregenza, J. Twelftree, C. Hulston, A review of thermoelectric generators for waste heat recovery in marine applications, Sustainable Energy Technol. Assess. 59 (2023), https://doi.org/10.1016/j.seta.2023.103394.
[46] M. Piper, A. Olenberg, J.M. Tran, E.Y. Kenig, Determination of the geometric design parameters of pillow-plate heat exchangers, Appl. Therm. Eng 91 (2015) 1168–1175, https://doi.org/10.1016/j.applthermaleng.2015.08.097.

[47] M. Piper, A. Zibart, J.M. Tran, E.Y. Kenig, Numerical investigation of turbulent forced convection heat transfer in pillow plates, Int. J. Heat Mass. Transf. 94 (2016) 516–527, https://doi.org/10.1016/j.ijheatmasstransfer.2015.11.014.
[48] M. Piper, A. Zibart, E.Y. Kenig, New design equations for turbulent forced convection heat transfer and pressure loss in pillow-plate channels, Int. J. Therm. Sci. 120 (2017) 459–468, https://doi.org/10.1016/j.ijthermalsci.2017.06.012.
[49] M. Mastani Joybari, H. Selvnes, A. Sevault, A. Hafner, Potentials and challenges for pillow-plate heat exchangers: State-of-the-art review, Appl. Therm. Eng. 214 (2022), https://doi.org/10.1016/j.applthermaleng.2022.118739.
[50] A. Kumar, A. Kumar, Heat transfer analysis in thermal energy storage—A comprehensive review-based latent heat storage system, Energy Storage 5 (2023), https://doi.org/10.1002/est2.434.
[51] M. Tavallaei, M. Farzaneh-Gord, A.J. Moghadam, A. Ebrahimi-Moghadam, Parametric study and optimization of pillow-plate heat exchanger using multi-objective genetic algorithm and entropy generation minimization approaches, Heat and Mass Transfer/Waerme- Und Stoffuebertragung 59 (2023) 1687–1706, https://doi.org/10.1007/s00231-023-03363-x.
[52] L. Esteves, A. Magalhães, V. Ferreira, C. Pinho, Test of two phase change materials for thermal energy storage: Determination of the global heat transfer coefficient, Chem. Engineering 2 (2018) 1–16, https://doi.org/10.3390/chemengineering2010010.
[53] L. Ciappi, P. Niknam, R. Fisher, A. Sciacovelli, Application of Flat Plate Latent Heat Thermal Energy Storage for Waste Heat Recovery and Energy Flexibility in Maritime Sector, in: 36th International Conference on Efficiency, Cost, Optimization, Simulation and Environmental Impact of Energy Systems (ECOS 2023), ECOS 2023, Las Palmas De Gran Canaria, Spain, 2023, pp. 2342–2353, https://doi.org/10.52202/069564-0211.
[54] M. Fadl, P.C. Eames, Numerical investigation of the influence of mushy zone parameter Amush on heat transfer characteristics in vertically and horizontally oriented thermal energy storage systems, Appl. Therm. Eng. 151 (2019) 90–99, https://doi.org/10.1016/j.applthermaleng.2019.01.102.
[55] V.R. Voller, C. Prakash, A fixed grid numerical modeing methodology for convection-diffusion mushy region phase-change problems, 1987.
[56] ANSYS Incorporated, ANSYS Fluent Theory Guide, (2021).
[57] B.E. Launder, D.B. Spalding, Lectures in Mathematical Models of Turbulence, Academic Press, London, England, 1972.
[58] F. Fornarelli, S.M. Camporeale, B. Fortunato, M. Torresi, P. Oresta, L. Magliocchetti, A. Miliozzi, G. Santo, CFD analysis of melting process in a shell-and-tube latent heat storage for concentrated solar power plants, Appl. Energy 164 (2016) 711–722, https://doi.org/10.1016/j.apenergy.2015.11.106.
[59] J. Wołoszyn, K. Szopa, G. Czerwiński, Enhanced heat transfer in a PCM shell-and-tube thermal energy storage system, Appl. Therm. Eng. 196 (2021) 117332, https://doi.org/10.1016/j.applthermaleng.2021.117332.
[60] G. Humbert, C. Roosendaal, J.K. Swanepoel, H.M. Navarro, W.G. Le Roux, A. Sciacovelli, Development of a latent heat thermal energy storage unit for the exhaust of a recuperated solar-dish Brayton cycle, Appl. Therm. Eng. 216 (2022), https://doi.org/10.1016/j.applthermaleng.2022.118994.
[61] PCM Products Ltd, PlusICE® Range, (n.d.). https://www.pcmproducts.net/files/PlusICE%20Range%202021-1.pdf (accessed March 10, 2023).
[62] Rubitherm Technologies GmbH, PCM RT-Line, (n.d.). https://www.rubitherm.eu/en/productcategory/organische-pcm-rt (accessed March 10, 2023).
[63] J.C. Helton, F.J. Davis, Latin hypercube sampling and the propagation of uncertainty in analyses of complex systems, Reliab. Eng. Syst. Saf. 81 (2003) 23–69, https://doi.org/10.1016/S0951-8320(03)00058-9.
[64] D. Guarda, G. Righetti, G.A. Longo, C. Zilio, S. Mancin, Experimental assessment of low temperature phase change materials (PCM) for refrigerating and air conditioning applications, Int. J. Refrig 154 (2023) 33–42, https://doi.org/10.1016/j.ijrefrig.2023.07.016.
[65] J. Lizana, M. de-Borja-Torrejon, A. Barrios-Padura, T. Auer, R. Chacartegui, Passive cooling through phase change materials in buildings. A critical study of implementation alternatives, Appl Energy 254 (2019), https://doi.org/10.1016/j.apenergy.2019.113658.
[66] J. Lizana, C. Bordin, T. Rajabloo, Integration of solar latent heat storage towards optimal small-scale combined heat and power generation by Organic Rankine Cycle, J. Energy Storage 29 (2020), https://doi.org/10.1016/j.est.2020.101367.
[67] N.B. Desai, M.E. Mondejar, F. Haglind, Techno-economic analysis of two-tank and packed-bed rock thermal energy storages for foil-based concentrating solar collector driven cogeneration plants, Renew. Energy 186 (2022) 814–830, https://doi.org/10.1016/j.renene.2022.01.043.
[68] R. Agathokleous, G. Bianchi, G. Panayiotou, L. Arestia, M.C. Argyrou, G. S. Georgiou, S.A. Tassou, H. Jouhara, S.A. Kalogirou, G.A. Florides, P. Christodoulides, Waste heat recovery in the EU industry and proposed new technologies, in: Energy Procedia, Elsevier Ltd, 2019, pp. 489–496, https://doi.org/10.1016/j.egypro.2019.02.064.
[69] S. Lion, I. Vlaskos, R. Taccani, A review of emissions reduction technologies for low and medium speed marine Diesel engines and their potential for waste heat recovery, Energy Convers. Manag. 207 (2020) 112553, https://doi.org/10.1016/j.enconman.2020.112553.
[70] F. Baldi, F. Ahlgren, T. Van Nguyen, M. Thern, K. Andersson, Energy and exergy analysis of a cruise ship, Energies (basel) 11 (2018), https://doi.org/10.3390/en11102508.
[71] International Maritime Organisation, IMO participation at COP 27, (2023).
[72] X. Guo, A.P. Goumba, C. Wang, Comparison of Direct and Indirect Active Thermal Energy Storage Strategies for Large-Scale Solar Heating Systems, Energies (basel) 12 (2019) 1948, https://doi.org/10.3390/en12101948.
[73] P.H. Niknam, R. Fisher, L. Ciappi, A. Sciacovelli, Optimally integrated waste heat recovery through combined emerging thermal technologies: Modelling, optimization and assessment for onboard multi-energy systems, Appl. Energy 366 (2024) 123298, https://doi.org/10.1016/j.apenergy.2024.123298.
[74] M. Longeon, A. Soupart, J.-F. Fourmigué, A. Bruch, P. Marty, Experimental and numerical study of annular PCM storage in the presence of natural convection, Appl. Energy 112 (2013) 175–184, https://doi.org/10.1016/j.apenergy.2013.06.007.
[75] J. Vogel, J. Felbinger, M. Johnson, Natural convection in high temperature flat plate latent heat thermal energy storage systems, Appl. Energy 184 (2016) 184–196, https://doi.org/10.1016/j.apenergy.2016.10.001.
[76] H. Qu, M.H. Masud, M. Islam, M.I.H. Khan, A.A. Ananno, A. Karim, Sustainable food drying technologies based on renewable energy sources, Crit. Rev. Food Sci. Nutr. 62 (2022) 6872–6886, https://doi.org/10.1080/10408398.2021.1907529.
[77] H. Chirino, B. Xu, X. Xu, Parametric study of cascade latent heat thermal energy storage (CLHTES) system in Concentrated Solar Power (CSP) plants, J. Energy Inst. 92 (2019) 653–664, https://doi.org/10.1016/j.joei.2018.03.007.
[78] G. Shen, X. Wang, J. Yu, Y. Bin, S. Zhong, S. Yang, J. Wang, Experimental investigation of thermal performance of vertical multitube cylindrical latent heat thermal energy storage systems, Environ. Sci. Pollut. Res. (2024), https://doi.org/10.1007/s11356-024-31864-7.
[79] M. Kabbara, D. Groulx, A. Joseph, Experimental investigations of a latent heat energy storage unit using finned tubes, Appl Therm Eng 101 (2016) 601–611, https://doi.org/10.1016/j.applthermaleng.2015.12.080.
[80] G.K. Marri, R. Srikanth, C. Balaji, Effect of phase change and ambient temperatures on the thermal performance of a solid-liquid phase change material based heat sinks, J. Energy Storage 30 (2020), https://doi.org/10.1016/j.est.2020.101327.
[81] N. Lakshmi Narasimhan, G. Srinivasan, Analysis of a thermal storage unit containing multiple phase change materials dispersed with high conductivity particles, J. Mech. Sci. Technol. 32 (2018) 373–380, https://doi.org/10.1007/s12206-017-1237-3.
[82] J. Zeng, W. Chen, W. Yu, L. Lyu, W. Luo, S. Xue, Application analysis of organic rankine cycle technology to recover ship waste heat and construction of experimental bench, in: 2022 IEEE 7th International Conference on Power and Renewable Energy, ICPRE 2022, Institute of Electrical and Electronics Engineers Inc, 2022, pp. 1063–1068, https://doi.org/10.1109/ICPRE55555.2022.9960614.
[83] Wärtsilä, Wärtsilä solutions for marine and oil & gas markets, n.d.
[84] F. Bentivoglio, S. Rouge, O. Soriano, A. Tempass de Sousa, Design and operation of a 180 kWh PCM heat storage at the Flaubert substation of the Grenoble urban heating network, Appl. Therm. Eng. 185 (2021), https://doi.org/10.1016/j.applthermaleng.2020.116402.
[85] H. Nazir, M. Batool, F.J. Bolivar Osorio, M. Isaza-Ruiz, X. Xu, K. Vignarooban, P. Phelan, A.M.K. Inamuddin, Recent developments in phase change materials for energy storage applications: A review, Int. J Heat Mass. Transf. 129 (2019) 491–523, https://doi.org/10.1016/j.ijheatmasstransfer.2018.09.126.
[86] Sunamp Ltd, Sunamp Thermino 300e Heat Battery, (n.d.). https://www.theheatpumpwarehouse.co.uk/shop/heat-batteries/sunamp-heat-batteries/sunamp-thermino-300-e-heat-battery/ (accessed March 21, 2024).
[87] IEA-ETSAP, IRENA, Thermal Energy Storage Energy Technology Systems Analysis Programme, 2013. www.etsap.org-www.irena.org.
[88] P. Pallis, E. Varvagiannis, K. Braimakis, T. Roumpedakis, A.D. Leontaritis, S. Karellas, Development, experimental testing and techno-economic assessment of a fully automated marine organic rankine cycle prototype for jacket cooling water heat recovery, Energy 228 (2021), https://doi.org/10.1016/j.energy.2021.120596.
[89] M. Herrera Rodriguez, P.J. Agrell, C. Manrique-de-Lara-Peñate, L. Trujillo, A multi-criteria fleet deployment model for cost, time and environmental impact, Int J Prod Econ 243 (2022), https://doi.org/10.1016/j.ijpe.2021.108325.
[90] Marine Insight, What is TEU in Shipping – Everything You Wanted to Know, (2022). https://www.marineinsight.com/maritime-law/teu-in-shipping-everything-you-wanted-to-know/ (accessed March 6, 2024).
[91] N.K. Park, S.K. Park, A study on the estimation of facilities in LNG bunkering terminal by Simulation-Busan port case, J Mar Sci Eng 7 (2019), https://doi.org/10.3390/jmse7100354.
[92] T. Cepowski, P. Chorab, The use of artificial neural networks to determine the engine power and fuel consumption of modern bulk carriers, tankers and container ships, Energies (basel) 14 (2021), https://doi.org/10.3390/en14164827.
[93] J. Marzi, A. Papanikolaou, J. Brunswig, J. Marzi, A. Papanikolaou, J. Brunswig, P. Corrignan, L. Lecointre, A. Aubert, G. Zaraphonitis, S. Harries, HOLISTIC ship design optimisation, 2018. https://www.researchgate.net/publication/325595000.
[94] United Nations Conference on Trade and Development, Review of maritime transport 2022, United nations, 2023.
[95] Equasis, The 2022 World Merchant Fleet, n.d.